https://doi.org/10.5194/essd-2026-449
Preprint. Discussion started: 2 September 2026

Open Access Earth System Science Data Discussions

A compiled dataset of Greenland weather station observations and reconstructed surface air temperature

Shujing Wang[1], Yetang Wang[1*], Yulun Zhang[1], Zhaosheng Zhai[1], Shugui Hou[2]

[1] College of Geography and Environment, Shandong Normal University, Jinan 250014, China

[2] Key Laboratory of Coast and Island Development of Ministry of Education, School of Geography and Ocean Science, Nanjing University, Nanjing, China

Corresponding to: Yetang Wang (yetangwang@sdnu.edu.cn)

Abstract. Climate variability is a main driver of mass imbalance of the Greenland Ice Sheet. However, quantitative assessments of climate change in this region are constrained by the sparseness, heterogeneity, and discontinuity of in situ measurements, imposing significant challenges to reliable modelling and future projections. To address this, we compile all available weather station observations over Greenland from 1941 to present into a single and standardized dataset at both daily and monthly temporal resolutions. This dataset includes seven climate variables: temperature, wind speed, wind direction, relative humidity, radiation, precipitation, and pressure, which is accessible at https://doi.org/10.11888/Atmos.tpdc.303490 (Wang and Wang, 2026). All data were harmonized and processed by a uniform quality control procedure, with the outliers flagged. For each station, detailed metadata covering source, location, and data availability are supplied. The dataset facilitates a thorough analysis of multi-variable climate characteristics in Greenland and can be used for the validation of global reanalysis products, regional climate models and remote sensing retrievals as well as data assimilation and climate reconstruction. Furthermore, we use the temperature observations from the compiled dataset together with a digital elevation model and ERA5 reanalysis to reconstruct a high-resolution (0.1°) monthly surface air temperature (SAT) dataset for Greenland (1950–2024), based on the optimized method identified after comparing five distinct machine learning models. The resulting SAT reconstruction exhibit a great improvement over ERA5, reducing the root mean square error (RMSE) by more than 60% and increasing squared correlation coefficient (R^2) by 5%. The high accuracy of this reconstruction is further confirmed by spatial cross-validation across 11 distinct regional divisions. The reconstruction is also publicly available at the Third Pole Environment Data Center (https://doi.org/10.11888/Cryos.tpdc.303026, Wang and Wang, 2025).

https://doi.org/10.5194/essd-2026-449
Preprint. Discussion started: 2 September 2026

1 Introduction

The Greenland Ice Sheet (GrIS) play a crucial role in regulating Earth's climate by altering atmospheric circulation patterns through surface albedo feedbacks, acting as a large cold source of the global atmosphere, and influencing oceanic currents via the influx of freshwater of melting ice (e.g., Noël et al., 2021; IPCC, 2021). Since the 1990s, the ice sheet has been experiencing an accelerated mass loss primarily driven by increased surface meltwater runoff (e.g., The IMBIE Team, 2020). This establishes it as a critical tipping element within the climate system (e.g., Lenton et al., 2008, 2019) and a dominant contributor of contemporary global sea level rise (Golledge et al., 2019; Box et al., 2022). The surface mass balance of an ice sheet is jointly governed by both surface energy and hydrological cycles, which involves complex, nonlinear interactions among temperature, radiative fluxes, wind speed and additional meteorological factors (e.g., Konzelmann and Braithwaite, 1995; Bonsoms et al., 2024). To robustly estimate the sensitivity of the GrIS surface mass balance to climate change, high-quality, long-term observational records are an indispensable foundation. Among the climatic variables, temperature serves as a core driver of surface ablation flux, with its spatiotemporal variability directly regulating the mass loss from the GrIS (Hanna et al., 2021; Beckmann and Winkelmann, 2023; IPCC, 2021). Furthermore, an accurate reconstruction of surface air temperature (SAT) variations across the entire Greenland likewise relies on the availability of the aforementioned observational data.

The oldest instrumental meteorological records over Greenland date back to the second half of the 18th century, but they extend for no more than nine years (Przybylak et al., 2024). Since the late 19th or early 20th centuries, more than ten staffed coastal weather stations provide continuous meteorological records of 30 years or longer, which were compiled by the Danish Meteorological Institute (DMI; John Cappelen (ed), 2014). From the 1980s onwards, a number of automatic weather stations (AWSs) have been installed by DMI, the University of Wisconsin-Madison, the Institute for Marine and Atmospheric research Utrecht (IMAU) of Utrecht University, and the Meteorological Research Institute (MRI) at the Japan Meteorological Agency, etc. Specially, two major AWS observational networks, i.e., Programme for Monitoring of the GrIS (PROMICE) and Greenland Climate Network (GC-Net) have been established. Despite extensive efforts made to monitor the GrIS atmospheric variables through staffed and automatic weather stations, observations still suffer from temporal discontinuity and sparse coverage across certain glaciological zones. Moreover, these observational data from different institutions,

https://doi.org/10.5194/essd-2026-449
Preprint. Discussion started: 2 September 2026

different periods, and in various formats have long remained scattered, lacking systematic compilation, quality control, and standardized integration. In recent years, several efforts have been made to compile and harmonize meteorological observations from Greenland and the broader Arctic region, but most have targeted specific networks or regions (e.g., Smeets et al., 2018; Vandecrux et al., 2023; Nishimura et al., 2023c; Fausto et al., 2026). Most recently, Rasmussen et al. (2025) assembled a pan-Arctic terrestrial AWS observation dataset that includes Greenland, but it is primarily confined to 1990–2023. Although this dataset encompasses Greenland stations, its original design targeting the entire Arctic region does not fully resolve Greenland's station density and spatial heterogeneity. While these compilation efforts have improved data accessibility, none has yet provided a unified, long-term, multi-variable dataset with consistent quality control specifically tailored to Greenland. Therefore, a comprehensive compilation of all weather station observations over Greenland, spanning a longer time period and coupled with data quality control using consistent criteria, is still needed.

Spatially and temporally complete datasets of climatic variables, especially SAT, are essential for robustly estimating total surface meltwater across the GrIS and characterizing the atmosphere–surface energy exchange. Numerical simulations offer a direct approach to this goal. Global reanalysis products and regional climate models can reproduce year-to-year variability and even long-term trends in Greenland climate change. Nevertheless, substantial biases in magnitude and spatial variations still exist (Huai et al., 2020; Zhang et al., 2021). An alternative approach is to use ground-based observations as the primary constraint and employs methods such as statistics or machine learning to extrapolate discrete station data into a continuous spatial domain. Early studies primarily employed statistical methods, such as bias correction (Box et al., 2009), kriging interpolation (Cowtan and Way, 2014), and data interpolating empirical orthogonal functions (Huang et al., 2017). However, these statistical prediction methods generally rest on linear or stationarity assumptions. In reality, the climate system is dynamic and exhibits nonlinear behaviour. As a result, such methods fail to adequately capture nonlinear relationships among different variables and are unable to represent extreme events effectively (Von Storch et al., 2004; Christiansen and Ljungqvist, 2017). In recent years, machine learning has demonstrated its strengths in modeling nonlinear relationships and complex interactions. (Karpatne et al., 2019). This capability has promoted its application in Arctic temperature reconstructions (e.g., Che et al., 2022; Vandecrux et al., 2024; Ma et al., 2025). However, regardless of whether statistical methods or machine learning are used, the accuracy of the reconstruction depends on the quality, coverage, and

https://doi.org/10.5194/essd-2026-449
Preprint. Discussion started: 2 September 2026

temporal extent of the input observational data. Therefore, based on a systematic compilation of historical station observations, the development of a long-term, high-resolution machine learning gridded dataset for Greenland has become a priority.

Our main objective is to compile all available scattered multi-source meteorological observations in Greenland, perform quality control on them, and to establish a standardized dataset of air temperature, surface pressure, wind speed, wind direction, relative humidity, radiation and precipitation at the daily and monthly resolutions since 1941. As a second data product derived from this compilation, we identified the optimal model by comparing five machine learning models and used it to reconstruct a monthly Greenland SAT dataset from 1950 to 2024. This reconstruction leverages the compiled temperature observations combined with ERA5 reanalysis and is accompanied by an uncertainty assessment.

2 Construction of the Greenland weather observation dataset

2.1 Data collection and sources

The weather station observations compiled in this study (Figure 1) are derived from multiple publicly available resources and are classified into three temporal resolutions: sub-daily, daily, and monthly. The sub-daily data include intervals of ten minutes, half-hour, hourly, three-hourly, and six-hourly, sourced from the Global Historical Climatology Network Hourly (GHCNh; Menne et al., 2024); the NOAA Global Monitoring Laboratory (GML) meteorological observations at Summit station; the National Centers for Environmental Information (NCEI) AWS at the fronts of Jakobshavn and Helheim glaciers (Holland and Holland, 2016a, b); the sub-daily data from the Institute for IMAU AWS network assembled by Smeets et al. (2018, 2022) and Van Tiggelen et al. (2024a, b) on PANGAEA; the AWS data measured by the Snow Impurity and Glacial Microbe effects on abrupt warming in the Arctic (SIGMA; Nishimura et al., 2023a, b and c); the three-hourly GRIP AWS data provided by the Antarctic Meteorological Research Center (AMRDC) of the University of Wisconsin–Madison (Antarctic Meteorological Research and Data Center, 1989, 1990); and the AWS and manual station observation data provided by the DMI (Danish Meteorological Institute, 2025). The daily data comprise the Climate History Network Daily (GHCNd; Menne et al., 2012a, b) records, the historical GISP AWS dataset archived by NOAA NCEI (Stearns and Weidner, 1997), the GC-Net Level 1 historical AWS data (Steffen

https://doi.org/10.5194/essd-2026-449
Preprint. Discussion started: 2 September 2026

Earth System Science Data
Open Access
Discussions

et al., 2022; Vandecrux et al., 2023) , and daily observations from the PROMICE project (How et al., 2022; Fausto et al., 2026). Monthly data include the same PROMICE project monthly products (How et al., 2022; Fausto et al., 2026). It should be noted that for multiple source records from the same site, we have excluded those with identical content; where differences exist, we have supplemented and merged the information from the different sources. The measurement instrumentation and associated uncertainties for each contributing network are summarized in Table A2.

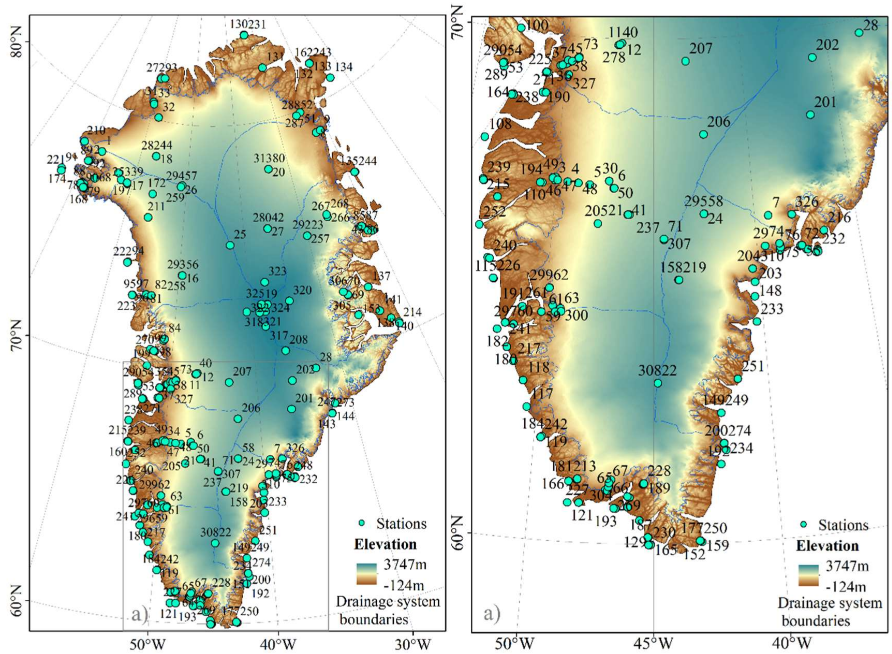

Figure 1. A map showing the distribution of the 327 weather stations included in this study; the black numbers (1–327) correspond to the "NO." column in Table A1, while the blue numbers correspond to the 11 designated river basins (Zwally et al., 2012).

2.2 Data processing

2.2.1 Averaging procedure

Since the original data have varying temporal resolutions, records already at daily or monthly resolution are directly included in the corresponding daily or monthly products. For data with higher (sub-daily) temporal resolution, they are uniformly aggregated to generate daily and monthly data. In all aggregation procedures, an 80% threshold for valid data is employed, and different averaging methods are used depending on the variable type: wind direction is averaged using circular mean (i.e., the mean angle of

https://doi.org/10.5194/essd-2026-449
Preprint. Discussion started: 2 September 2026

Open Access Earth System Science Data Discussions

the direction vectors) (Jammalamadaka and SenGupta, 2001), while all other variables are averaged using arithmetic mean.

When aggregating sub-daily data to daily data, the temporal resolution for each calendar day is first determined. Given that the same station may have inconsistent resolutions as a result of instrument upgrades or malfunctions, we calculate the hourly differences between consecutive observations to identify the data interval (e.g., 1-hour, 3-hour, or 6-hour intervals) and subsequently compute the expected number of complete data points for that day (e.g., 48 points for half-hourly resolution, 24 points for hourly resolution, 8 points for 3-hourly resolution, and 4 points for 6-hourly resolution). In cases where only a single data point is available on a given day, its resolution cannot be inferred, and it is consequently flagged as missing. For each meteorological variable, the number of valid observations on that day is counted, and its proportion relative to the expected total number of points is calculated. The daily average for a variable is computed only when the number of valid data points reaches at least 80% of the expected total points; otherwise, the daily average is recorded as missing.

When aggregating daily data to monthly data, the actual number of days in each month is first determined (accounting for leap years), and the number of valid daily values for each variable within that month is then counted. The monthly average for a variable is computed only when the count of valid daily values constitutes at least 80% of the total days in that month; otherwise, the monthly average is set to missing.

Through these procedures, complete daily and monthly products are ultimately generated. These products include the variables listed in Table 1.

It should be noted that the compiled dataset in this study includes sub-daily observations with varying native sampling frequencies. As pointed out by Rapp et al. (2026) for Greenland climate records, aggregating such observations into daily or monthly means may introduce systematic biases in the estimated averages due to uneven sampling intervals. To mitigate this issue as far as possible, we applied a threshold requiring that valid observations constitute at least 80% of the expected total for a given temporal resolution when calculating daily means. This procedure partially suppresses the sampling bias arising from uneven temporal coverage, but it cannot completely eliminate the uncertainties induced by differences in sampling frequencies across various data sources. Users should be aware that for daily-scale analyses or for early period station records with sparse temporal coverage, such sampling related uncertainties may still exist.

https://doi.org/10.5194/essd-2026-449
Preprint. Discussion started: 2 September 2026

Open Access Earth System Science Data Discussions

Table 1. A summary of all variables in the data product.

Element	Variable	Variable Description
Temperature	tem	Average temperature
	tem_i	Average temperature (instantaneous)
	tem_l	Average temperature (lower boom)
	tem_u	Average temperature (upper boom)
	tem_2	Average temperature (2 m)
	tem_cs500_l	Air temperature (Vaisala CS500 sensor) (lower boom)
	tem_cs500_u	Air temperature (Vaisala CS500 sensor) (upper boom)
Wind Speed	wind speed	Mean wind speed
	Wind speed_i	Mean wind speed (instantaneous)
	Wind speed_l	Mean wind speed (lower boom)
	Wind speed_u	Mean wind speed (upper boom)
	Wind speed_10	Mean wind speed (10 m)
	Wind (max) speed	Peak gust wind speed
	wind speed(x)_u wind speed(y)_u	Directional wind speed from direction x/y (upper boom)
	wind speed(x)_l wind speed(y)_l	Directional wind speed from direction x/y (lower boom)
	wind speed(x)_i wind speed(y)_i	Directional wind speed from direction x/y (instantaneous)
Wind Direction	wind direction	Wind direction
	Wind direction_i	Wind direction (instantaneous)
	Wind direction_l	Wind direction (lower boom)
	Wind direction_u	Wind direction (upper boom)
	Wind direction_10	Wind direction (10 m)
	Wind（max) direction	Direction of peak wind gust
Relative Humidity	RH	Mean relative humidity
	RH_u	Relative humidity (upper boom)
	RH_l	Relative humidity (lower boom)
	RH_i	Relative humidity (instantaneous)
	RH_2	Relative humidity (2 m)
	RH_ice_u	Relative humidity (upper boom)-adjusted for saturation over ice in subfreezing conditions
	RH_ice_l	Relative humidity (lower boom)-adjusted for saturation over ice in subfreezing conditions
	RH_ice_i	Relative humidity (instantaneous)-adjusted for saturation over ice in subfreezing conditions
Radiation	DSR	Downwelling shortwave radiation
	DSR_cor	Downwelling shortwave radiation-tilt-corrected from DSR
	USR	Upwelling shortwave radiation

https://doi.org/10.5194/essd-2026-449
Preprint. Discussion started: 2 September 2026

	USR_cor	Upwelling shortwave radiation-tilt-corrected from USR
	DLR	Downwelling longwave radiation
	ULR	Upwelling longwave radiation
Pressure	pressure	Air pressure
	pressure_u	Air pressure (upper boom)
	pressure_l	Air pressure (lower boom)
	pressure_i	Air pressure (instantaneous)
Precipitation	Precipitation	Precipitation
	Precipitation_u_cor	Corrected cumulative liquid precipitation (upper boom)
	Precipitation_l_cor	Corrected cumulative liquid precipitation (lower boom
Sensor	sensor_height_l	Height of the lower boom of the sensor
	sensor_height_u	Height of the upper boom of the sensor

2.2.2 Quality control

Most of the observational data we have collected have already been subjected to quality control by the data providers. To generate a high-quality unified dataset, we performed additional uniform quality checks on the data (Table 2), referring to the quality control methodologies of existing datasets (Wang et al., 2023; Nishimura et al., 2023c; Rasmussen et al., 2025). These checks include basic cleaning: standardizing measurement units, eliminating invalid placeholders (e.g., "9999"), and establishing physical thresholds to remove extreme outliers that clearly violate physical principles. They also incorporate mutation analysis and statistical analysis. For daily products, we compare each value with the monthly mean of the same month and examine abrupt changes between consecutive days. For monthly products, we check for abrupt changes between the same months of adjacent years; pronounced fluctuations are flagged as suspected anomalies (which may stem from instrument malfunctions, data entry errors, or genuine extreme weather events). We apply the three-sigma (3σ) rule to identify statistical outliers that significantly deviate from the monthly climatological background. To further eliminate outliers and enhance dataset reliability, we visually cross-compared each filtered time series with the corresponding ERA5. Finally, all anomalous data are flagged but not deleted. This approach preserves the complete raw dataset while allowing us to distinguish between potentially erroneous data and genuine extreme weather events, which can be filtered or used as needed in subsequent steps.

Table 2. Details of the quality checks performed on each variable and the conditions set.

Category	unit	QC Rule	Daily Data	Monthly Data	Flag Bit
Temperature	°C	Climatological range check	> 60 °C or < −80 °C (during months 6, 7, 8, and 9: < −40 °C)		1

https://doi.org/10.5194/essd-2026-449
Preprint. Discussion started: 2 September 2026

		Mean comparison	Deviation from monthly mean > 20 °C	Deviation from historical same-month mean > 15 °C	2
		Temporal consistency	|ΔT| between consecutive days > 25 °C	Adjacent-year same-month difference > 20 °C	4
		Three-sigma test	Outside monthly mean ± 3σ	Outside historical same-month mean ± 3σ	8
Wind Speed	m/s	Range check	< 0 m/s or > 100 m/s		1
		Consecutive identical values	> 3 consecutive days with identical values	> 3 consecutive months with identical values	2
		Three-sigma test	Outside monthly mean ± 3σ	Outside historical same-month mean ± 3σ	8
Wind Direction	°	Range check	< 0° or > 360°		1
		Consecutive identical values	> 3 consecutive days with identical values	> 3 consecutive months with identical values	2
Relative Humidity	%	Range check	< 0 or > 100 or = 100		1
		Three-sigma test	Outside monthly mean ± 3σ	Outside historical same-month mean ± 3σ	8
Radiation	W/m²	Range check	≤ 0		1
		Three-sigma test	Outside monthly mean ± 3σ	Outside historical same-month mean ± 3σ	8
Pressure	hPa	Range check	< 650 hPa or > 1100 hPa		1
		Temporal consistency	|ΔP| between consecutive days > 30 hPa	Adjacent-year same-month difference > 25 hPa	4
		Three-sigma test	Outside monthly mean ±3σ	Outside historical same-month mean ± 3σ	8
Precipitation	mm	Range check	< 0 mm or > 3000 mm		1
		Consecutive identical values	—	> 3 consecutive months with identical values	2
		Three-sigma test	Outside monthly mean ± 3σ	Outside historical same-month mean ± 3σ	8

https://doi.org/10.5194/essd-2026-449
Preprint. Discussion started: 2 September 2026

3 Characteristics of the Greenland weather observation dataset

For the compiled daily data of various meteorological variables, we calculate the number of stations in each major category that provide at least one record per year (Figure 2), in order to represent the temporal density of data. The number of stations with records for each category shows an upward trend, with a notable increase beginning around 1995. Among all categories, In the later period, the number of temperature stations were the most numerous in the later period, which underscores the central role of temperature in climate monitoring. In contrast, the maximum number of stations with precipitation records in 2024 was only 45. It should be noted that these statistics merely reflect the number of stations with at least one record per year and do not indicate complete data coverage for any station throughout the entire year.

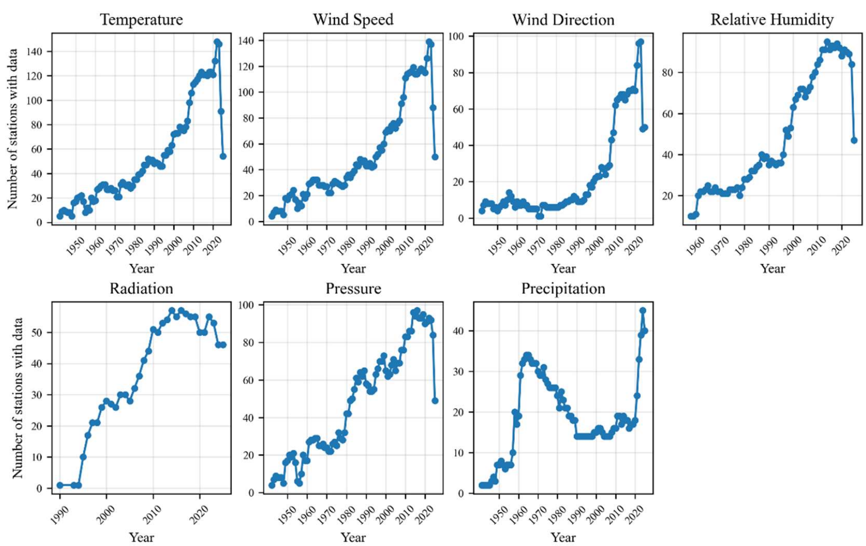

Figure 2. Annual station coverage by variable category.

Figure 3 and Figures A1–A6 present the data availability of daily temperature, wind speed, wind direction, relative humidity, radiation, pressure and precipitation. Among these variables, temperature has the highest average number of valid years (13.6 years), followed by wind speed (13.0 years) and pressure (12.2 years), indicating that the historical records for these three variables are relatively continuous. In contrast, radiation has the lowest average valid years (only 3.9 years), and precipitation is also low (4.8 years), which may be attributed to late initiation of observations or frequent interruptions. In terms of self-completeness rate, temperature (80.9%) and wind speed (78.4%) perform the best, suggesting that

https://doi.org/10.5194/essd-2026-449
Preprint. Discussion started: 2 September 2026

within their recorded periods, these two variables experienced fewer data collection interruptions and denser sampling. Conversely, radiation (25.0%) and precipitation (30.2%) have the lowest self-completeness rates. There are significant differences in the length of the observation history for each variable, and the number of observation stations was scarce in the early period, resulting in most stations covering only a segment of the time axis.

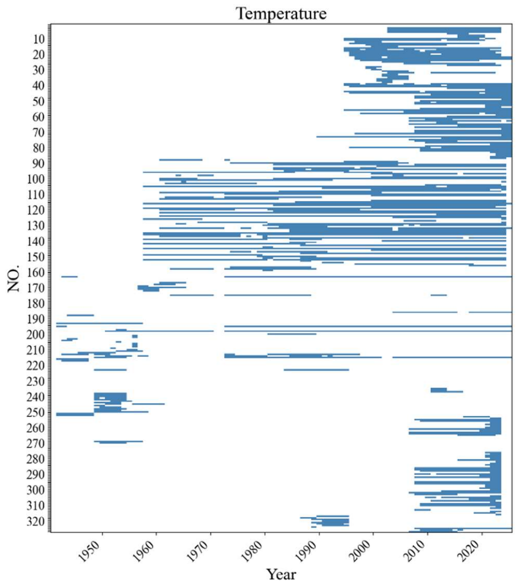

Figure 3. Daily data availability of temperature. Blue indicates that data is available, and 1–327 correspond to "NO." in Table A1.

We further examine spatial distribution of the number of valid data days for different meteorological categories across stations to reveal the actual recording conditions at various stations. The results (Figure 4) show that the number of valid data days for each meteorological category exhibits significant spatial differences and imbalances. Overall, for different variables, the number of valid recording days at per station is concentrated between 0 and 20,000 days, presenting a pattern of "more in the southwest coastal areas, less in the interior and the north". A few coastal stations maintain high numbers of valid days across multiple variables, with valid recording days reaching as high as 20,000 or more; In contrast, stations with long-term records are extremely rare in inland and northern regions, where most stations have fewer than 10,000 valid days, likely due to the harsh environment, logistical constraints, and difficulties in station maintenance leading to high data missing rates. Among the variables, temperature (275 stations) and wind speed (274 stations) have the widest station coverage. Radiation is the variable

https://doi.org/10.5194/essd-2026-449
Preprint. Discussion started: 2 September 2026

with the scarcest records, with data available from only 83 stations, and the number of valid days at all stations does not exceed 10,000. Although inland stations are few, their distribution is relatively “evenly” (sparsely distributed), unlike other variables that are concentrated along the coast. The distribution of precipitation stations shows the most significant north-south disparity, with 101 stations recording data, making it the variable with the second lowest data availability after radiation. This scarcity may be related to the ease of blockage of polar rain gauges and their high heating power consumption (Rasmussen et al., 2012). Overall, the number of stations with complete data for multiple variables in Greenland is extremely limited.

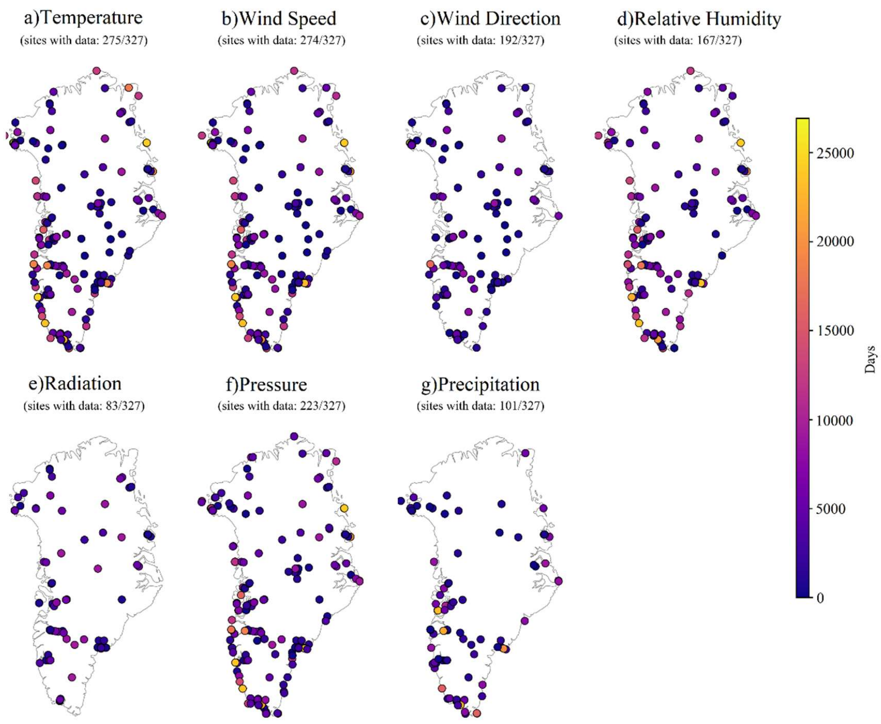

Figure 4. Spatial distribution of valid data days across meteorological categories at Greenland stations.

4 Overview of the Greenland weather observation dataset

4.1 Multiyear daily average of the climate variable

We selected at least one representative variable for each element and calculated the daily average values of that variable at each station over the period 1990–2025 (Figure 5). The overall results are significantly influenced by altitude, latitude, and sea-land distribution. The 2-meter temperature (tem_2) exhibits a

https://doi.org/10.5194/essd-2026-449
Preprint. Discussion started: 2 September 2026

latitudinal pattern of being higher in the south and lower in the north, with average temperatures mostly above 0 °C in the south and below −15 °C in the northern tip. Meanwhile, due to high altitude and high ice-sheet albedo in the interior, contrasting with low altitude, exposed ground that absorbs more heat, and the moderating effect of the ocean in coastal areas, the tem_2 shows a notable pattern of higher values along the coast and lower values inland. Surface wind speed over Greenland exhibits significant spatial heterogeneity, controlled jointly by the katabatic wind system, topographic slope, ice surface conditions, and large-scale atmospheric circulation (Stearns et al., 1997; Gorter et al., 2014). Wind speed in the x-direction is higher (positive) in the west and lower (negative) in the east, while in the y-direction it shows the opposite pattern: lower (negative) in the west and higher (positive) in the east; the prevailing wind direction is concentrated between 100° and 250°. Because of the low temperatures in Greenland, water vapor in the air is close to condensation, and clear-sky precipitation occurs in the interior (Cox et al., 2019; Guy et al., 2023), resulting in relatively high humidity relative to liquid water, generally above 65%. The four radiation components (DSR, USR, DLR, ULR) are mainly influenced by solar radiation, temperature, and cloud cover (Li et al., 2023; Kawaguchi et al., 2024). In coastal areas, water vapor transported inland is easily blocked by topography to form clouds, which suppress DSR and consequently reduce USR; therefore, shortwave radiation is lower along the coast than inland. Longwave radiation is more significantly affected by cloud cover, exhibiting a pattern of higher values along the coast and lower values inland, especially in southwestern and southeastern Greenland. Cyclonic activity in the Baffin Bay region and the Icelandic Low in the southeast transport water vapor into the interior of Greenland, where it condenses into clouds and precipitation, increasing longwave radiation and resulting in higher longwave radiation values in these areas. Pressure is dominated by altitude differences and decreases with increasing elevation, reaching up to 1000 hPa at low-elevation coastal sites and below 700 hPa at high-elevation inland sites. Precipitation measurement stations are mainly located in coastal areas, with few stations inland; the daily average precipitation is generally below 0.5 mm.

https://doi.org/10.5194/essd-2026-449
Preprint. Discussion started: 2 September 2026

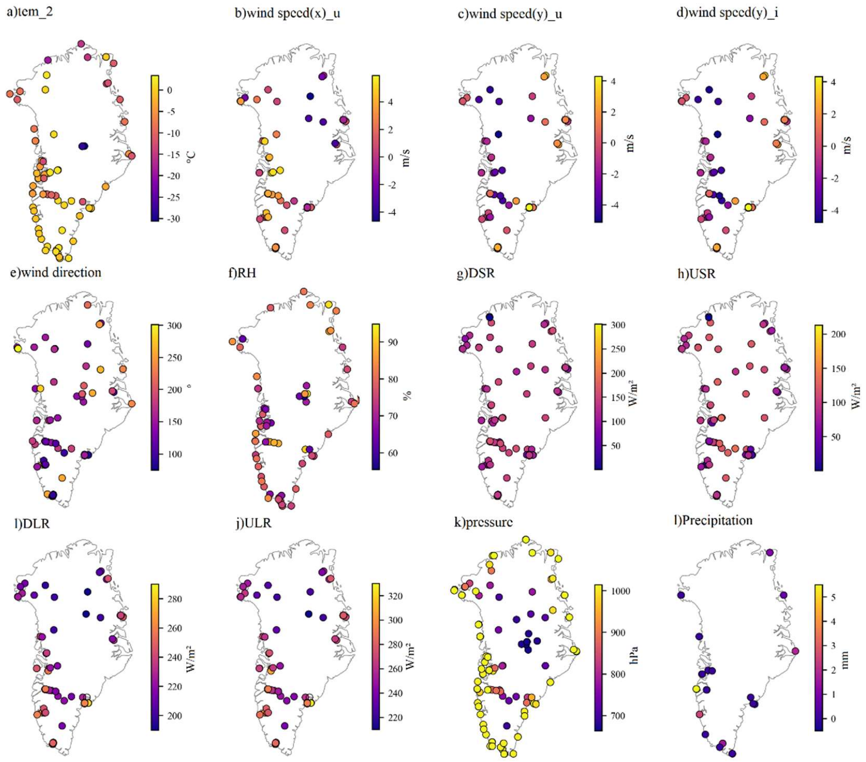

Figure 5. Spatial distribution of the multiyear (1990–2025) daily mean of the representative variable for each element (temperature, wind speed, wind direction, relative humidity, radiation, pressure, precipitation) at weather stations.

4.2 Climatology at the sites of the Greenland weather station observation dataset

Using the Greenland weather station observation dataset, we selected nine stations with over ten years of valid data for each of the two variables (2-meter air temperature and air pressure). To ensure data representativeness, each of these two station groups included three stations situated on the GrIS. We then analyse their climatic variations throughout the year. The 2-meter air temperature exhibits significant seasonal variations and a strong latitudinal gradient (Figure 6). In terms of the climatological mean state, northern coastal sites such as Danmarkshavn and Daneborg are characterized by a "long, bitterly cold season and a short, cool warm season". During the cold season, temperatures remain below 0 °C and can drop to below −20 °C; the period with temperatures above 0 °C in the warm season lasts only about three months, with maximum average temperatures around 5–8 °C. Consequently, the annual temperature range exceeds 25 °C. In contrast, southern coastal stations like Qaqortoq and Narsarsuaq experience more

https://doi.org/10.5194/essd-2026-449
Preprint. Discussion started: 2 September 2026

moderate temperature variations. Average cold season temperatures hover around −5 °C, while the warm season features nearly 200 days with temperatures above 0 °C and maximum average temperatures reaching 7–10 °C. Moving inland from the ice sheet margin (GRL_S5 and GRL_S10) to the central Summit site, temperatures exhibit a clear decreasing trend. In winter, enhanced radiative cooling at Summit drives minimum temperatures below −40 °C, and consequently yields a larger annual range (~30 °C) compared to the marginal sites. Summer differences are equally striking, Summit peaks at only −12 °C and remains below freezing year-round, whereas GRL_S5 and GRL_S10 experience brief excursions above 0 °C, suggesting a seasonal melting potential. Furthermore, the interannual variability of winter temperatures is significantly larger than that of summer at all stations. Compared with 2-meter air temperature, seasonal variation of air pressure is relatively moderate. Although some seasonal fluctuations exist at each station, the overall signal is weak. In terms of annual range, ice sheet sites (about 30 hPa) show significantly larger variations than coastal sites (15–20 hPa). The three representative ice sheet sites (Tunu-N, NASA-E, and Saddle) all display a typical seasonal pattern, with higher pressure in summer and lower in winter, reflecting the amplifying effect of high-altitude regions on seasonal thermal changes. Regarding absolute pressure levels, ice sheet sites have markedly lower values, ranging between 700 and 800 hPa; in contrast, the coastal stations Danmarkshavn and Daneborg have the highest annual mean pressure, with climatological averages remaining above 1010 hPa.

https://doi.org/10.5194/essd-2026-449
Preprint. Discussion started: 2 September 2026

Open Access Earth System Science Data Discussions

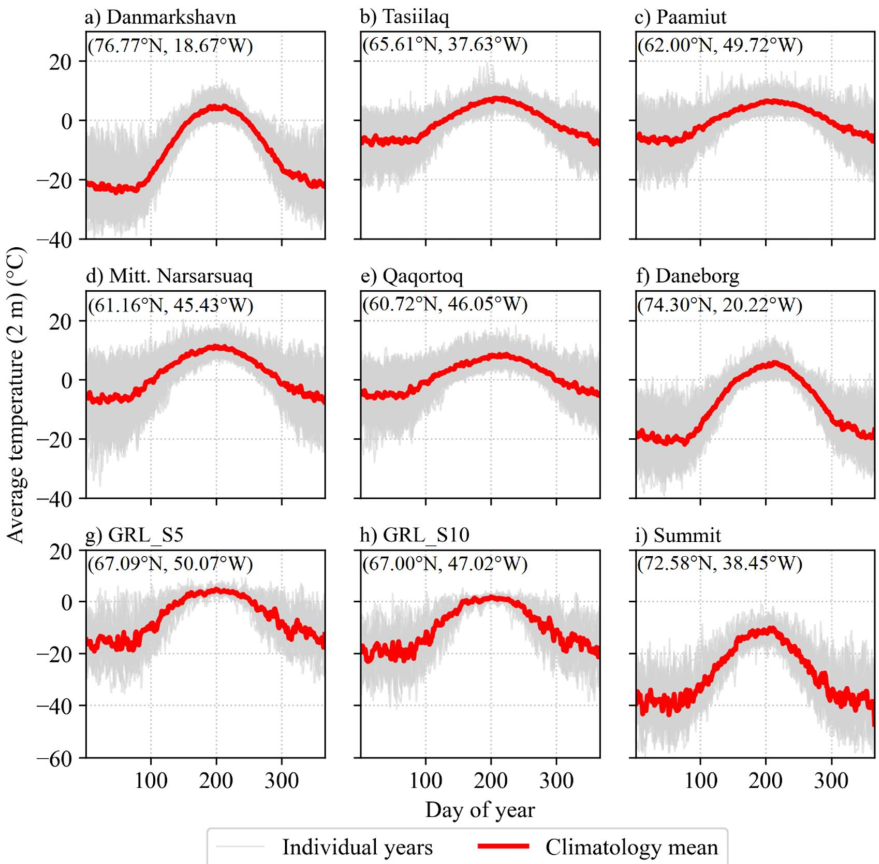

290

Figure 6. Climatology of daily average temperature at 2 meters.

https://doi.org/10.5194/essd-2026-449
Preprint. Discussion started: 2 September 2026

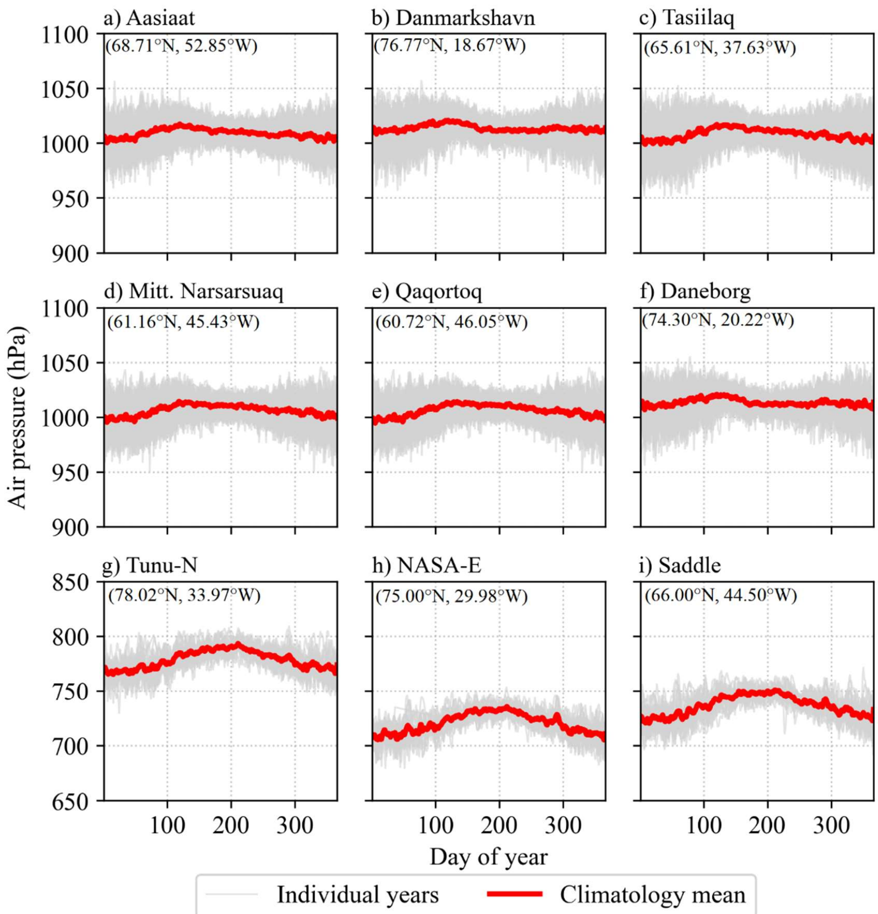

Figure 7. Climatology of daily air pressure.

5 Gridded SAT reconstruction dataset

5.1 Data used for reconstruction

Beside the monthly SAT station observations from our constructed dataset, we use ERA5, which is the fifth-generation reanalysis product generated by the European Centre for Medium-Range Weather Forecasts (ECMWF), using the Cy41r2 version of the Integrated Forecasting System (IFS) combining with four-dimensional variational assimilation (4D-Var) (Hersbach et al., 2020). It spans from January 1940 to present at a horizontal resolution of 0.25° × 0.25°. ERA5-Land is a land surface reanalysis dataset that utilizes ERA5 reanalysis data as the meteorological forcing field to force the ECMWF land surface process model HTESSEL for higher-resolution global numerical integration. Compared to ERA5, this

https://doi.org/10.5194/essd-2026-449
Preprint. Discussion started: 2 September 2026

dataset enhance the horizontal resolution (0.1° × 0.1°) through physics-based dynamic downscaling, enabling more accurate simulation of land surface variables such as surface temperature (Muñoz-Sabater et al., 2021). We utilized the monthly mean reanalysis 2m temperature, pressure, and wind speed data from ERA5-Land (1950–2024) as input features for model training. For decadal sliding average prior to 1949, we bilinearly interpolated the ERA5 data during 1940–1949 to 0.1° × 0.1° grid.

SAT changes are strongly influenced by topographic relief (Rolland, 2003; Mutiibwa et al., 2015). To improve the model performance for SAT, we use Greenland digital elevation model (DEM) data, from the National Tibetan Plateau Data Center (TPDC) (https://doi.org/10.11888/Geogra.tpdc.271336). The DEM has a resolution of 500 m (Fan et al., 2022). It is bilinearly resampled to 0.1°×0.1° to match the ERA5-land dataset.

5.2 Methods

5.2.1 Machine Learning Models

To evaluate the effectiveness of different algorithms for SAT reconstruction, we compared five representative machine learning models. These models include a hybrid model called LSTM-CNN, which combines convolutional neural network (CNN) and long short-term memory network (LSTM) to exploit the local feature extraction strengths of CNNs (Zhao et al., 2017) and the sequential modeling advantages of LSTM (Hochreiter and Schmidhuber, 1997; Yu et al., 2019; Sherstinsky, 2020); a hybrid model combining CNN with Transformer encoder (Transformer-CNN) (Vaswani et al., 2017); SoftRandomForest, a neural network model inspired by the Random Forest algorithm (Biau and Scornet, 2016; Breiman, 2001) that improves predictive performance by replacing traditional random decision trees with neural network-based soft decision trees and averaging the outputs of multiple such trees; SoftXGBoost, a boosting model based on soft decision tree (Chen and Guestrin, 2016) that extends the gradient boosting framework with differentiable tree structures; and an artificial neural network (ANN), which possesses strong nonlinear fitting capabilities and adaptability for handling complex meteorological data relationships (Cybenko, 1989; Hornik et al., 1989). The specific parameter configurations of these models are provided in the Appendix.

Since LSTM-CNN and Transformer-CNN incorporate early stopping mechanisms, data were randomly split into 86% (training), 4% (validation), and 10% (testing) sets. To maximize utilization of limited observational data, the remaining three models employed an 86% (training) and 14% (testing) split. The

https://doi.org/10.5194/essd-2026-449
Preprint. Discussion started: 2 September 2026

Open Access Earth System Science Data Discussions

validation and test sets are collectively referred to as the unseen data as they were not directly involved in training. Input features for all models were standardized. A repeated training strategy (10 independent runs) was employed to obtain stable performance evaluations, with average results used for model comparisons.

5.2.2 Input feature selection

According to the existing studies (Mutiibwa et al., 2015; Szymanowski and Kryza, 2017; Johnstone and Sulungu, 2021; Hou et al., 2023), and correlation analyses (Table 3), we find that among the candidate variables, the 2-meter air temperature (t2m) exhibited the highest correlation with the target variable at 0.98. The next highest correlations were observed for month, surface pressure, elevation, wind direction, latitude, amplitude of t2m, and longitude. However, due to its excessively low correlation with the target variable, longitude was excluded. To capture long-term and recent variability, we further included the past 10-year and past 3-year running means of temperature, pressure, and wind speed, along with values from the same month in the preceding year. Thus, the model has 22 input characteristic variables: temporal averages of air temperature, surface pressure, and wind speed over the preceding 10, 3, 2, and 1 years; their monthly values for the current and preceding year; and the annual amplitude of t2m, elevation, latitude, and month cosine value. The "month cosine value" refers to the cosine transformation applied to the monthly sequence of a year to encode seasonal cycles as a continuous variable. calculated as

$$month\_cos = cos\left(\frac{2\pi(m-1)}{12}\right) \tag{1}$$

where m represents the month index (1 represents January, 2 represents February, ..., 12 represents December).

Table 3. Correlations between the target variable (temperature, tem) at the observed data points and the variables in the ERA5, including t2m, surface pressure (sp), wind speed (ws), as well as elevation (dem), longitude, latitude, monthly cosine (month) and amplitude of t2m (t2m_amp) in the previous year.

Correlation	tem	month	t2m_amp	t2m	sp	ws	dem	latitude	longitude
r	1.00	−0.66	−0.27	0.98	0.54	−0.51	−0.53	−0.42	−0.07

https://doi.org/10.5194/essd-2026-449
Preprint. Discussion started: 2 September 2026

5.2.3 Reconstruction processing

Our reconstruction involves three key steps: processing input data, selecting the optimal model, and performing the final reconstruction (Figure 8). We began by filtering the compiled monthly temperature observations for Greenland. Exclude observation stations located outside the land boundaries of the main island of Greenland. We retain only stations with a continuous record length of at least two years between 1950 and 2024. Through correlation analysis, we selected key variables as input variables. Secondly, the input dataset was resampled to the site location and divided into training, test, and validation sets. Model performance was evaluated using the average root mean square error (RMSE), mean deviation (MD), and squared coefficient (R^2) on both training and unseen data. All five candidate models underwent ten rounds of iterative training and tuning until achieving "good" performance (RMSE<2.50 °C; $R^2 \geq 0.97$; MD<0.50). The model achieving the best performance on unseen data was selected for the final reconstruction across Greenland. Finally, the entire dataset of integrated input fields from the first step was fed into the optimal model (ANN) for SAT reconstruction, and then its uncertainty are estimated by a spatial cross-validated method.

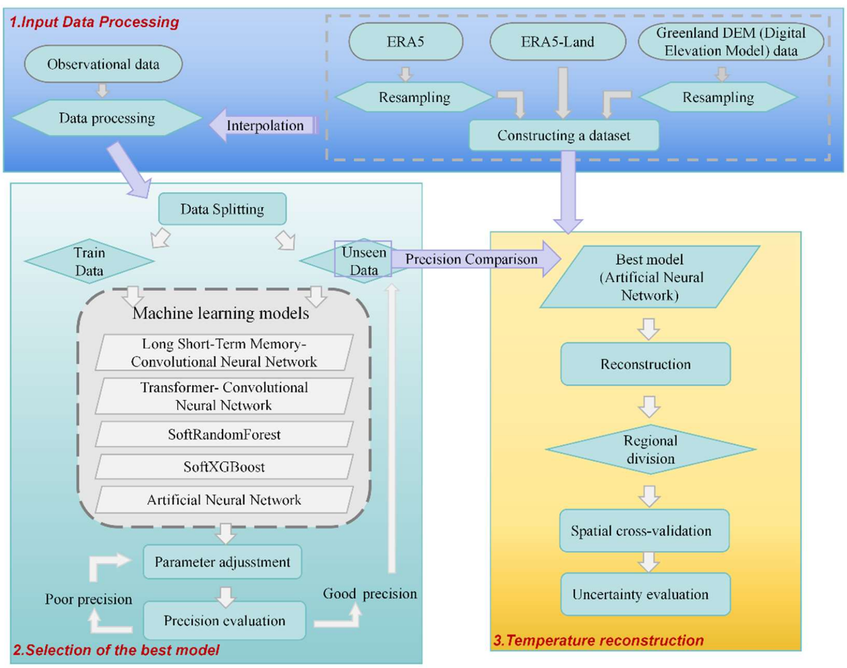

Figure 8. A chart of Greenland temperature reconstruction processes including input data processing (blue), selection of the best model (green), and temperature reconstruction (orange).

https://doi.org/10.5194/essd-2026-449
Preprint. Discussion started: 2 September 2026

5.2.4 Reconstruction accuracy assessment

Three standard metrics including RMSE, MD and R^2 are used for the estimation of the reconstruction accuracy. To compare the relative performance of the five candidate models for the GrIS SAT reconstruction, each model was trained ten times, and the average of RMSE, MD, and R^2 values were calculated against both the training data and test data (the latter not used in training, referred as unseen data).

We used a spatial cross-validation approach to assess the generalization ability of the selected best model across unseen regions (Brenning, 2012). The entire Greenland was divided into 11 sub-regions using drainage basins defined by Zwally et al. (2012). First, each observation station is assigned to its corresponding sub-region using spatial connectivity analysis. Subsequently, 11 rounds of iterative training are conducted. In each round, one sub-region is excluded, and the station within that sub-region are treated as an independent validation set, while the ANN model is trained using observation data from the remaining 10 sub-regions. During training, both the model and normalized parameters were saved simultaneously to ensure subsequent predictions employed statistical parameters from the training set for data transformation, maintaining consistency in preprocessing. Upon model completion, SAT predictions were generated for the excluded subregion (i.e., “unseen data”), with results stored. This process ensured each point received a prediction from a model that had never encountered its specific region, guaranteeing “spatial independence” in forecasting. Through this process, the study constructed 11 mutually independent ANN models. Finally, we input the entire region's feature quantities into each of the 11 models for prediction. The predicted mean serves as the SAT estimation, while the predicted standard deviation quantifies model uncertainty.

5.3 Comparison of five machine learning models for Greenland SAT reconstruction

Accuracy assessments (Figure 9) shows that the ratio of the predictions of each machine learning model to observations tends to approach unity, with data points clustered along the 1:1 trend line. R^2 values between predictions and observations for each model exceed 0.97. Among them, the ANN achieves the highest accuracy, with R^2 values of 0.99 for both training and unseen data, and RMSE values below 1.35 °C. The LSTM-CNN ranks second, with predictions that correlate significantly with the training observations (R^2 =0.99) and an RMSE as low as 1.01 °C. However, its performance declines for the unseen data, where it achieves an R^2 of 0.98 and an RMSE of 1.58 °C, indicating weaker generalization compared to the ANN. The SoftRandomForest shows the lowest predictive accuracy among the five models, with an R^2 of only 0.97, and RMSE values of above 2 °C for both the training and unseen datasets. Transformer-CNN outperforms slightly SoftXGBoost, yielding RMSE values of 1.68 °C on the training set and 1.69 °C on the unseen dataset.

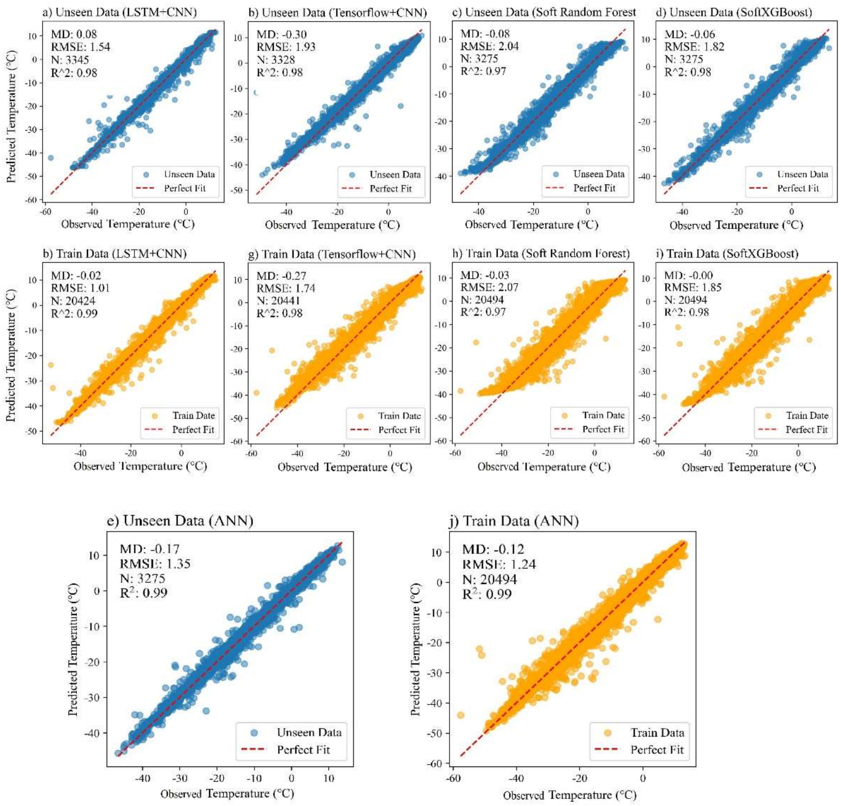

Figure 9. Accuracy comparison of LSTM-CNN (a, f), Transformer-CNN (b, g), SoftRandomForest (c, h), SoftXGBoost (d, i), and ANN (e, j) for unseen (a–e) and training (f–j) datasets. The root mean square error (RMSE), mean deviation (MD), and squared correlation coefficient (R^2) between the observed and predicted data, and the number of samples (N) are reported for each case.

5.4 Uncertainty of the ANN-based SAT reconstruction

Spatial cross-validation demonstrates ANN model achieves relatively robust generalization performance for monthly SAT over most of Greenland (Figure 10). Uncertainty, however, varies spatially, generally lower inland and higher along parts of the coast. Notably, elevated uncertainty is concentrated in the Disko Island region and along the coastal belt extending from northern Greenland to Cape Brewster.

https://doi.org/10.5194/essd-2026-449
Preprint. Discussion started: 2 September 2026

Along the northern coast, uncertainty peaks during the transitional months of May and September, potentially due to strong surface heterogeneity from snowmelt and sea-ice breakup, together with amplified local SAT variability caused by rapid phase changes in the surface energy balance (e.g., albedo feedback and freeze-thaw processes). Uncertainty varies little seasonally, indicating stable model performance. In all months and regions, the standard deviation of uncertainty remains below 2.4 °C.

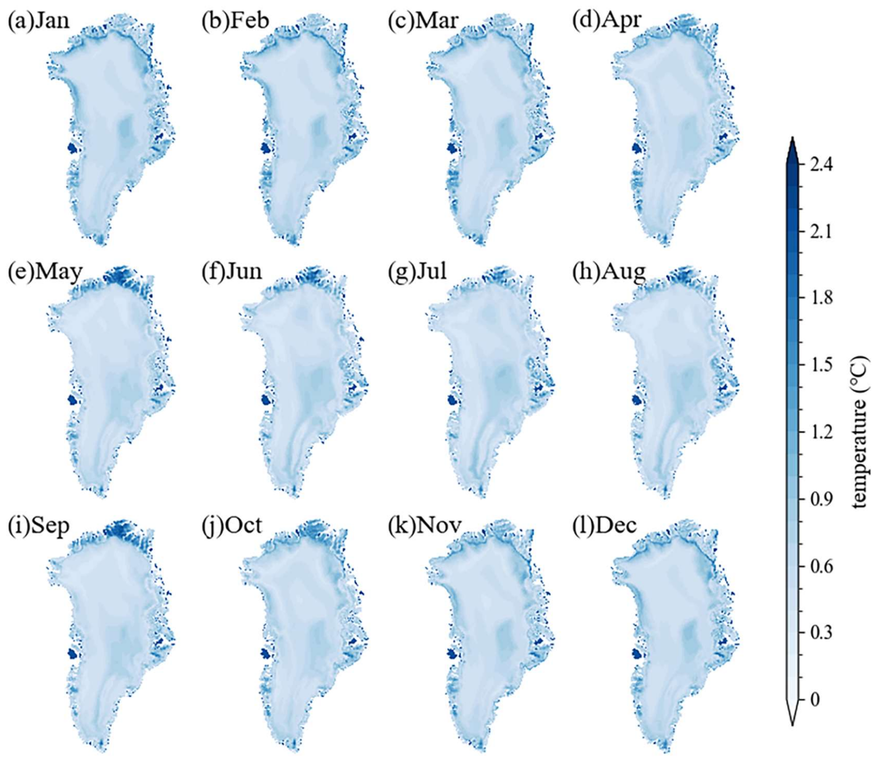

Figure 10. Spatial distribution of the mean ANN uncertainty from January to December for the period 1950–2024, calculated as the standard deviation of ANN predictions from 11 spatially cross-validated subsets.

Figure 11 presents the validation results of the reconstructed dataset and ERA5 products against station observations. The reconstructed dataset demonstrates extremely high accuracy, with an R^2 of 0.99, an RMSE of only 1.25 °C, and an MD of −0.16 °C. In contrast, ERA5 exhibits a pronounced systematic warm bias (MD = 1.31 °C) and greater dispersion (RMSE = 3.14 °C, R^2 = 0.94). Compared to ERA5, the reconstructed dataset achieves a reduction in RMSE of over 60% and an increase in R^2 of about 5%, showing a significant improvement in systematic bias while maintaining good consistency. These results indicate that, while preserving spatial continuity, the reconstructed dataset markedly improves the

https://doi.org/10.5194/essd-2026-449
Preprint. Discussion started: 2 September 2026

accuracy of temperature estimation, providing more reliable temperature field data for regional-scale high-resolution climate research.

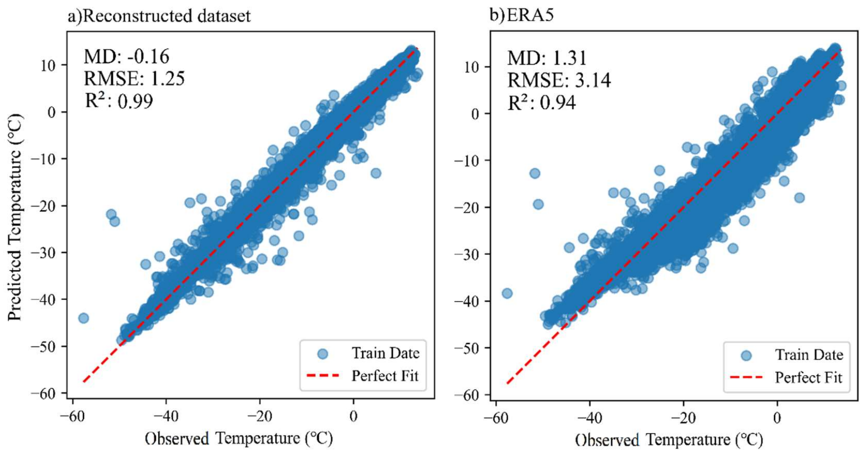

Figure 11. Validation of SAT (a) from the reconstructions and (b) ERA5, respectively, against station observations.

To compare the spatial climatological characteristics of the reconstructed data and ERA5 over Greenland, we first calculated the multi-year mean annual temperature fields from both datasets for the period 1950–2024. The two fields were then merged to obtain a joint average over the entire study region, which served as a unified reference. From this, we derived the anomaly fields for the reconstructed data and ERA5 separately, and the final bias field was defined as the reconstruction anomaly minus the ERA5 anomaly. Spatially, the anomaly fields of the reconstruction (Figure 12a) and ERA5 (Figure 12b) exhibit consistency, both clearly capturing the typical thermal pattern of "cold anomalies over the interior ice sheet and warm anomalies along the coastal margins" over Greenland. The cold center is located over the central ice sheet at the highest elevations, while the warm centers are mainly distributed along the southwestern and southeastern coastal zones. This indicates that, while inheriting the large-scale spatial continuity of ERA5, the reconstruction achieves finer spatial detail through its higher resolution. The bias field (Figure 12c) further reveals systematic differences between the two datasets. Over the high-altitude interior of the GrIS, the bias field shows extensive negative values, indicating that the reconstruction is colder than ERA5. In contrast, along parts of the southwestern, southern, and eastern coastal areas, pronounced positive values are evident, indicating that the reconstruction is warmer than ERA5. This alternating positive–negative bias pattern is highly consistent with the finding of Zhang et

https://doi.org/10.5194/essd-2026-449
Preprint. Discussion started: 2 September 2026

al. (2021) that ERA5 exhibits a significant warm bias in the accumulation zone and a cold bias in the ablation zone over the GrIS. By comparison, the reconstruction effectively suppresses the warm bias of ERA5 in the accumulation zone and substantially raises temperature estimates in the ablation zone, thereby correcting the cold bias of ERA5.

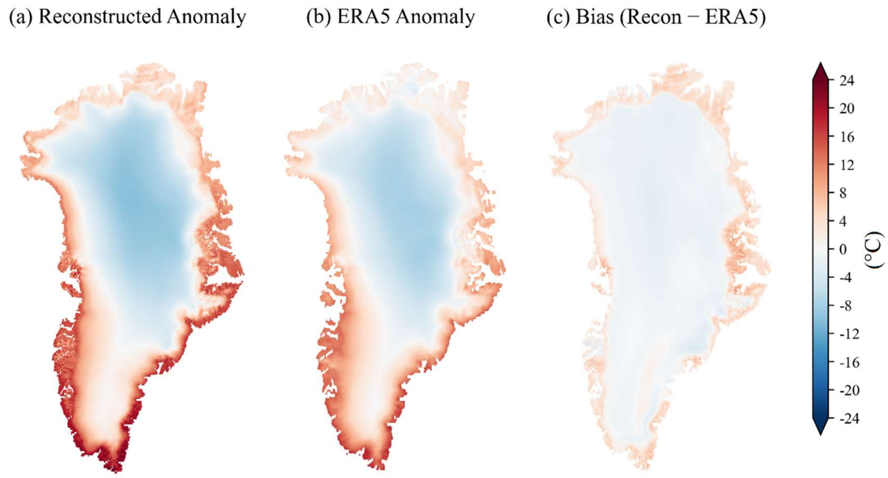

Figure 12. Comparison of temperature anomalies between the reconstruction and ERA5 and their bias over Greenland (1950–2024).

5.5 Presentation of reconstructed Greenland SAT

The average SAT at each month from the reconstruction shows a spatial gradient of decrease from the ice sheet periphery to the central north (Figure 13). In winter (December–February), the entire Greenland is below 0 °C, with minimum SAT reaching below −42 °C. Greenland warms up gradually in spring (March–May), and regions with SAT above 0 °C first emerge along the southern coast. In March, the entire region remains below freezing, with a maximum temperature of −1.37 °C. By April and May, maximum SAT exceed 0 °C, reaching about 2.76 °C in April and 6.88 °C in May, respectively, while the above-freezing region along the southern coast expands. During the summer months (June–August), SAT values remain below 0 °C in the interior but exceeded freezing along the coast. The warmest month is July, with maximum values around 12.15 °C. During autumn (September–November), SAT gradually decrease across Greenland, and the area of positive temperatures along the southern coast decreases.

https://doi.org/10.5194/essd-2026-449
Preprint. Discussion started: 2 September 2026

Open Access Earth System Science Data Discussions

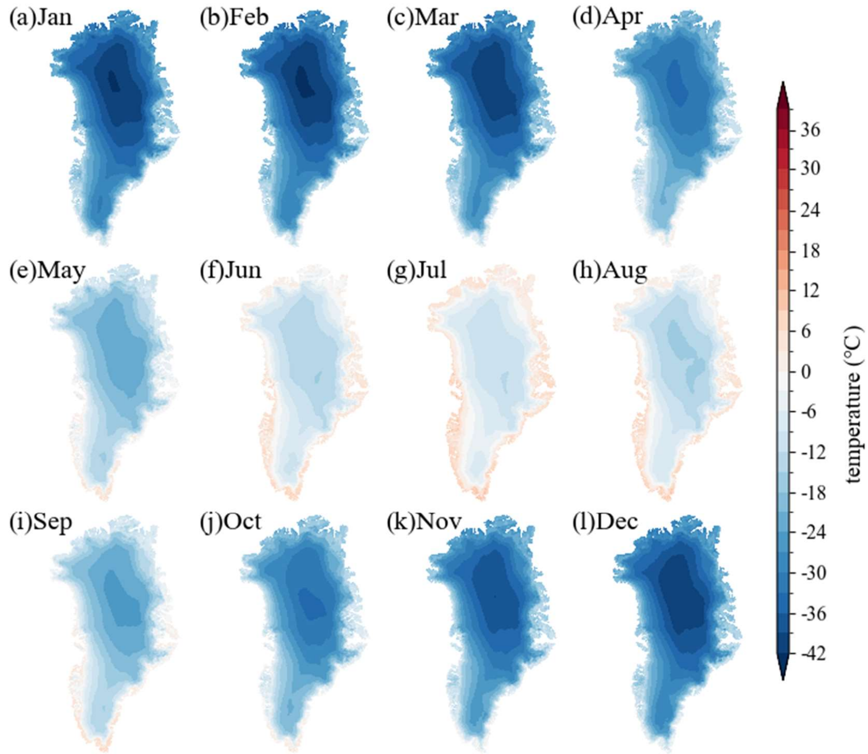

Figure 13. Spatial distribution of mean monthly temperatures from January to December over the period 1950–2024, from the reconstruction.

Spatial patterns of SAT trends across Greenland for each month from 1950 to 2024 is shown in Figure 14. In winter, widespread warming in December weakens from northwest to southeast, despite localized cooling along the northern coast. January and February show pronounced inland cooling but strong coastal warming, with the strongest warming anomalies occurring along the northern ice sheet edge. Meanwhile, a small area between the ice sheet edge and the coast experienced cooling. In spring, March shows northwest warming and southeast cooling, with localized cooling persisting along the northern coast. By April, warming prevails across most of Greenland, weakening south-eastward, while cooling is limited to small coastal areas in the north and southwest. May exhibits weak, spatially widespread but insignificant cooling, although northern regions continue to warm. During summer and autumn, spatial differences in trends are modest.

https://doi.org/10.5194/essd-2026-449
Preprint. Discussion started: 2 September 2026

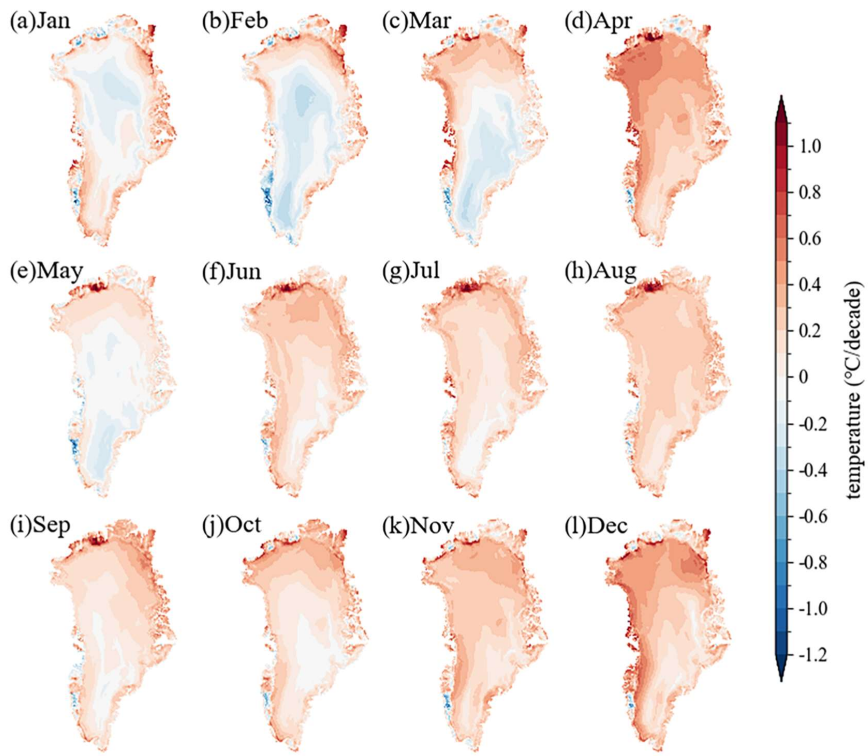

Figure 14. Monthly SAT trends from January to December temperatures from the reconstruction during 1950–2024.

6 Discussion and Conclusions

We present a comprehensive compilation of long-term meteorological measurements across Greenland. This compiled dataset encompasses seven essential variables: air temperature, wind speed, wind direction, relative humidity, radiation, precipitation, and air pressure. These variables are recorded at daily and monthly frequencies, accompanied by detailed metadata regarding the source, geographic location, and data availability for each station. A unified quality control framework has been applied to the collected data, with anomalous entries flagged to streamline subsequent analyses. Compared with the pan-Arctic weather dataset recently compiled by Rasmussen et al. (2025), our dataset specially focuses on Greenland, augmenting additional meteorological variables (e.g., wind speed, wind direction, and pressure), extending the temporal coverage, and incorporating a denser network of observational stations. Among the seven variables, radiation and precipitation are the two with the fewest observation stations. Notably, several stations located in the southeastern coastal region maintain a high number of valid record days across multiple variables. Reanalysis datasets, satellite retrieval products and regional climate models often display biases over the GrIS, particularly in complex terrain such as glacial valleys and coastal steep slopes. To quantify these biases, this dataset can serve as an independent validation source (e.g., Adolph et al., 2018; Huai et al., 2020; Zhang et al., 2021; Covi et al., 2025). Furthermore, given the lack of long-term continuous observations across most of Greenland, this dataset provides a critical foundation for climate reconstruction when combined with alternative data sources or methods such as statistical downscaling and machine learning. It also strengthens the comprehensive understanding and analytical capability of Greenland's multivariate climatic characteristics.

Moreover, we reconstruct monthly mean SAT over Greenland for the period 1950–2024 using compiled temperature observations and 22 ERA5 and DEM variables. Five machine learning models were trained; the ANN yielded the highest predictive accuracy for unseen data, achieving a RMSE of 1.35 °C, and thus was selected to reconstruct SAT at 0.1° resolution. Spatial cross-validation indicates lower uncertainty inland and slightly higher values along coastlines, with overall uncertainty below 2.4 °C. This new Greenland SAT dataset holds substantial potential for advancing Arctic research. Potential applications include quantifying warming trends of large spaces and long timescales, reducing uncertainties in melt-runoff estimates (Colosio et al., 2020; Li et al., 2024), and facilitating more detailed mechanistic analyses of ice sheet dynamics.

The weather station network in Greenland remains incomplete, suffering from temporal discontinuities and uneven spatial distribution. In particular, most of the northern inland areas are undocumented. Future efforts should prioritize the expansion of station coverage in the northern region and the interior, although the installation and maintenance of meteorological observation stations in such extreme environments pose considerable challenges. Furthermore, observations of precipitation and radiation need to be significantly strengthened, as only a small number of stations are currently capable of providing these measurements. It is worth noting that some recently deployed weather stations, including those operated by Chinese institutions, are not included in the current compilation due to data accessibility restrictions or limited temporal coverage. As the weather station network continues to develop and we progressively incorporate these newly deployed stations, and as data are updated on an ongoing basis, we will further enhance the dataset by adopting stricter quality control procedures to identify and flag hidden errors in

https://doi.org/10.5194/essd-2026-449
Preprint. Discussion started: 2 September 2026

the raw data. Moreover, we will assign detailed quality flags to each observation, thereby enabling users to assess data reliability and facilitating more accurate climate analyses and model validation.

Appendix A

Table A1. Compiled site information. Please note that the information in this table is sourced from official documents (# Suppl. GC-Net Level 1; ## Suppl. GHCN-Hourly; ### Suppl.GHCN-Dail; #### Suppl. GHCN-Hourly and GHCN -Daily).

No.	Station	Lat (°)	Lon (°)	Ele(m)	Source
1	SIGMA-A	78.05	-67.63	1490	SIGMA (Nishimura et al., 2023a, c)
2	SIGMA-B	77.52	-69.06°	944	SIGMA (Nishimura et al., 2023b, c)
3	GRL_S5	67.09	-50.07	490	IMAU (Smeets et al., 2022; Van Tiggelen et al., 2024a)
4	GRL_S6	67.08	-49.41	1020	IMAU (Smeets et al., 2022; Van Tiggelen et al., 2024a)
5	GRL_S9	67.05	-48.27	1520	IMAU (Smeets et al., 2022; Van Tiggelen et al., 2024a)
6	GRL_S10	67.00	-47.02	1840	IMAU (Smeets et al., 2022; Van Tiggelen et al., 2024a)
7	GRL_S21	66.36	-39.31	1615	IMAU (Van Tiggelen et al., 2024b)
8	GRL_S22	78.90	-22.38	535	IMAU (Van Tiggelen et al., 2024b)
9	GRL_S23	78.92	-21.45	142	IMAU (Van Tiggelen et al., 2024b)
10	Swiss Camp	69.56	-49.36	1138	GC-Net (Level 1 historical automated weather station) (Steffen et al., 2022; Vandecrux et al., 2023)
11	Crawford Point 1	69.87	-47.02	2022	
12	CP2	69.91	-46.85	1990	
13	JAR1	69.49	-49.71	900	
14	JAR2	69.42	-50.06	568	
15	JAR3	69.39	-50.31	323	
16	NASA-U	73.84	-49.53	2369	
17	GITS	77.14	-61.04	1887	
18	Humboldt	78.53	-56.84	1950	
19	Summit	72.58	-38.50	3254	

https://doi.org/10.5194/essd-2026-449
Preprint. Discussion started: 2 September 2026

20	Tunu-N	78.02	-33.97	2113	
21	DYE-2	66.48	-46.29	2165	
22	South Dome#	63.15	-44.82	2878	
23	NASA-E#	75.00	-29.98	2610	
24	NASA-SE	66.48	-42.50	2360	
25	NGRIP	75.10	-42.33	2950	
26	NEEM	77.44	-51.10	2460	
27	EastGRIP	75.63	-35.98	2653	
28	KAR	69.70	-33.00	2579	
29	KULU	65.76	-39.60	878	
30	Aurora	67.14	-47.29	1798	
31	Petermann Glacier	80.68	-60.29	37	
32	Petermann ELA	80.10	-58.15	907	
33	SMS-PET	80.60	-60.05	54	
34	SMS1	69.48	-49.80	822	
35	SMS2	69.48	-49.88	727	
36	SMS3	69.44	-49.97	605	
37	SMS4	69.40	-50.21	387	
38	SMS5	69.51	-49.91	—	
39	CEN	77.18	-61.11	1890	PROMICE and GC-Net (How, P. et al., 2022; Fausto et al., 2026)
40	CP1	69.87	-47.05	1954	
41	DY2	66.48	-46.30	2125	
42	EGP	75.63	-35.97	2668	
43	FRE	74.39	-20.83	683	
44	HUM	78.53	-56.85	1967	
45	JAR	69.49	-49.68	929	
46	KAN_B##	67.13	-50.18	350	
47	KAN_L	67.10	-49.94	684	
48	KAN_M	67.07	-48.86	1266	
49	KAN_T	67.15	-50.04	499	
50	KAN_U	67.00	-47.04	1849	
51	KPC_L	79.91	-24.08	358	
52	KPC_U	79.84	-25.16	868	
53	LYN_L##	69.32	-53.54	539	
54	LYN_T##	69.30	-53.59	944	
55	MIT	65.69	-37.83	425	
56	NAU	73.84	-49.54	2337	
57	NEM	77.44	-51.08	2456	
58	NSE	66.48	-42.49	2385	
59	NUK_B	64.46	-50.15	107	
60	NUK_K##	64.16	-51.36	700	
61	NUK_L	64.48	-49.52	558	
62	NUK_N##	64.95	-49.88	919	

https://doi.org/10.5194/essd-2026-449
Preprint. Discussion started: 2 September 2026

Open Access Earth System Science Data Discussions

63	NUK_U	64.51	-49.29	1110	
64	QAS_A##	61.24	-46.73	1003	
65	QAS_L##	61.03	-46.85	227	
66	QAS_M	61.11	-46.81	671	
67	QAS_U	61.17	-46.82	879	
68	RED_L	76.93	-66.96	768	
69	SCO_L	72.22	-26.82	435	
70	SCO_U	72.39	-27.21	965	
71	SDL#	66.00	-44.50	2474	
72	SER_B	65.68	-37.92	27	
73	SWC	69.59	-49.29	1152	
74	TAS_A	65.77	-38.89	876	
75	TAS_L	65.64	-38.90	226	
76	TAS_U	65.70	-38.87	569	
77	THU_L	76.40	-68.27	562	
78	THU_L2	76.39	-68.27	573	
79	THU_U	76.39	-68.11	745	
80	TUN	78.02	-33.96	2079	
81	UPE_L	72.89	-54.30	198	
82	UPE_U	72.88	-53.63	909	
83	WEG_B	71.14	-51.22	14	
84	WEG_L	71.20	-51.10	930	
85	ZAC_A	74.65	-21.65	1481	
86	ZAC_L	74.62	-21.37	626	
87	ZAC_U	74.64	-21.46	857	
88	04200 Dundas###	76.57	-68.80	21	DMI (Danish Meteorological Institute, 2025)
89	04201 Qaanaaq	77.47	-69.22	16	
90	04202 Pituffik###	76.53	-68.75	77	
91	04203 Kitsissut	76.73	-73.12	11	
92	04205 Qaanaaq###	77.48	-69.20	14	
	04205 Mitt. Qaanaaq	77.49	-69.37	16	
93	04207 Hall Land	81.68	-59.95	105	
94	04208 Kitsissorsuit	74.06	-57.72	40	
95	04209 Upernavik AWS	72.78	-56.17	63	
96	04210 Upernavik###	72.78	-56.17	63	
		72.78	-56.17	120	
97	04211 Mitt. Upernavik	72.79	-56.13	126	
98	04212 Uummannaq	70.67	-52.12	39	
	04212 Uummannaq Heli.	70.68	-52.12	15	
99	04213 Mitt. Qaarsut	70.73	-52.70	88	
		70.73	-52.70	88	
100	04214 Qullitsat####	70.05	-52.85	2	
	04214 Nuussuaq	70.66	-54.60	27	

https://doi.org/10.5194/essd-2026-449
Preprint. Discussion started: 2 September 2026

101	04216 Ilulissat###	69.22	-51.05	39
102	04217 Qasigiannguit	68.82	-51.08	77
103	04218 Qeqertarsuaq###	69.23	-53.52	24
104	04219 Qeqertarsuaq Heli.	69.25	-53.51	3
105	04220 Aasiaat	68.71	-52.85	43
106	04221 Mitt. Ilulissat	69.24	-51.07	29
107	04224 Mitt. Aasiaat	68.72	-52.78	23
108	04228 Kitsissut/Attu##	67.78	-53.97	12
		67.78	-53.96	10
109	04230 Sisimiut###	66.92	-53.67	12
110	04231 Mitt. Kangerlussuaq###	67.02	-50.70	50
	04231 Mitt. KangerlussuaqSAVS	67.01	-50.72	50
111	04234 Mitt. Sisimiut	66.95	-53.73	10
112	04235 Dye 1###	66.63	-52.87	1439
113	04240 Maniitsoq###	65.40	-52.87	25
114	04241 Mitt. Maniitsoq	65.41	-52.94	28
115	04242 Sioralik	65.01	-52.53	14
		65.01	-52.53	12
116	04250 Nuuk###	64.17	-51.75	25
		64.17	-51.75	54
		64.18	-51.73	80
117	04253 Ukiivik##	62.57	-50.42	22
		62.58	-50.41	20
118	04254 Qeqertarsuatsiaat	63.08	-50.68	—
	04254 Mitt. Nuuk	64.19	-50.68	87
119	04260 Paamiut	62.00	-49.72	15
	04260 Paamiut Heliport	62.00	-49.67	13
	04260 Mitt. Paamiut	62.01	-49.67	37
120	04261 Kangilinnguit	61.22	-48.12	27
		61.23	-48.10	35
121	04266 Nunarsuit	60.76	-48.45	33
		60.76	-48.45	31
122	04270 Mitt. Narsarsuaq	61.16	-45.43	34
123	04271 Narsarsuaq Radisonde	61.16	-45.44	4
124	04272 Qaqortoq###	60.72	-46.05	32
		60.72	-46.05	57
125	04273 Qaqortoq Heliport	60.72	-46.03	16
126	04280 Narsaq	60.90	-45.97	30
127	04282 Alluitsup PAA Helip.	60.46	-45.57	27
128	04283 Nanortalik	60.13	-45.22	21
129	04285 Angissoq	59.99	-45.11	20

https://doi.org/10.5194/essd-2026-449
Preprint. Discussion started: 2 September 2026

Open Access Earth System Science Data Discussions

		59.99	-45.15	14
130	04301 Kap Morris Jesup	83.65	-33.37	4
		83.66	-33.37	3
131	04305 Kap Harald Moltke##	82.15	-29.92	4
132	04310 Station Nord###	81.60	-16.65	36
133	04312 Station Nord AWS	81.60	-16.65	34
		81.60	-16.66	34
134	04313 Henrik Krøyer Holme	80.65	-13.72	10
		80.65	-13.71	8
135	04320 Danmarkshavn	76.77	-18.67	11
136	04330 Daneborg###	74.30	-20.22	12
		74.30	-20.22	44
		74.31	-20.22	13
137	04338 Mestersvig###	72.25	-23.90	16
138	04339 Ittoqqortoormiit	70.48	-21.95	65
		70.48	-21.95	70
139	04340 Uunarteq###	70.42	-21.97	42
		70.42	-21.97	41
140	04341 Mitt. Nerlerit Inaat	70.74	-22.65	14
141	04345 Jameson Land	71.18	-23.62	261
142	04350 Aputiteeq###	67.78	32.30	20
143	04351 Aputiteeq	67.78	-32.28	13
		67.78	-32.28	13
144	04352 Aputiteeq	67.78	-32.30	13
145	04360 Tasiilaq	65.61	-37.63	36
		65.60	-37.62	50
		65.61	-37.64	54
146	04361 Mitt. Kulusuk	65.57	-37.12	36
147	04365 DYE 4	65.53	-37.16	329
148	04373 Ikermit	64.78	-40.30	85
		64.78	-40.31	78
149	04380 Timmiarmiut###	62.53	-42.13	10
150	04381 Ikermiuarsuk	61.93	-42.07	39
151	04382 Ikermiuarsuk	61.94	-42.07	39
		61.94	-42.07	40
152	04390 Ikerasassuaq###	60.03	-43.12	75
		60.05	-43.17	26
		60.06	-43.17	88
		60.06	-43.17	140
153	04410 Renland	71.32	-26.32	2320
154	04415 Summit	72.58	-37.63	3250

https://doi.org/10.5194/essd-2026-449
Preprint. Discussion started: 2 September 2026

Open Access Earth System Science Data Discussions

155	04416 Summit	72.58	-38.45	3202	
156	04419 Summit Tower	72.57	-38.47	3209	
157	04465 DYE 2	66.48	-46.30	2332	
158	04475 DYE 3####	65.18	-43.83	2652	
159	04495 Ikerasassuaq	60.03	-43.12	26	
160	34234 Mitt. Sisimiut###	66.95	-53.72	10	
161	34250 Nuuk	64.18	-51.73	54	
162	34310 Station Nord	81.60	-16.66	36	
163	GLM00004220 AASIAAT (EGEDESMINDE)	68.70	-52.85	41	GHCN_daily (Menne et al., 2012a, b)
164	GLE00147001 AASIAAT	68.70	-52.75	43	
165	GLE00147361 ANGISOQ	59.98	-45.13	20	
166	GLE00147251 ARSUK	61.18	-48.45	-100	
167	GLW00017615 CAMP CENTURY##	77.17	-61.13	305	
168	GLW00017617 CAMP TUTO EAST ASC S##	76.38	-67.92	701	
169	GLW00017612 CAMP TUTO ICECAP ST##	76.42	-68.25	579	
170	GLW00017611 CAMP TUTO ICECAP STATION##	76.42	-68.32	488	
171	GLW00017614 CAMP TUTO ICECAP STATION##	76.40	-68.13	750	
172	GLW00017503 CAMP TUTO SITE 2##	76.98	-56.07	124	
173	GLW00017616 CAMP TUTO WEST ASC S	76.47	-68.67	305	
174	GL009012000 CAREY ISLANDS GREENLAND	76.73	-73.18	10	
175	GLE00147681 DYE 2##	66.48	-46.28	2332	
176	GLE00147571 DYE 4	65.52	-37.17	329	
177	GLE00147641 IKERASASSUAQ	60.05	-43.17	88	
178	GLE00146961 ILULISSAT	69.22	-51.10	39	
179	GLW00016404 IVIGTUT	61.22	-48.12	28	

https://doi.org/10.5194/essd-2026-449
Preprint. Discussion started: 2 September 2026

180	GLE00147191 KANGERLUARSORUSEQ	63.70	-51.55	10	
181	GLE00147241 KANGILINNGUIT	61.23	-48.10	35	
182	GLE00147181 KITSISSUT 1	64.03	-52.08	19	
183	GLE00147281 MITT. NARSARSUAQ	61.17	-45.42	27	
184	GLE00147231 MITT. PAAMIUT	62.02	-49.67	36	
185	GLE00146861 MITT. QAANAAQ	77.48	-69.38	16	
186	GLE00146908 MITT. UPERNAVIK	72.78	-56.13	126	
187	GLE00147351 NANORTALIK HELIPORT	60.13	-45.23	5	
188	GLE00147331 NARSAQ HELIPORT##	60.92	-46.05	25	
189	GLW00016405 NARSARSSUAK	61.18	-45.42	11	
190	GLE00146971 QASIGIANNGUIT HELI.	68.82	-51.17	24	
191	GLE00147141 QOORNOQ	64.53	-51.05	-100	
192	GLE00147631 QULLEQ	61.53	-42.23	157	
193	GLW00016407 SIMIUTAK##	60.68	-46.53	62	
194	GLW00016504 SONDRESTROM	67.02	-50.80	50	
195	GL000004360 TASIILAQ	65.60	-37.63	50	
196	GLW00017602 THULE	76.55	-68.82	38	
197	GLW00017610 THULE MILE 60 SIERRA##	77.23	-62.33	1704	
198	GLW00017605 PITUFFIK##	76.52	-68.83	77	
199	GLE00146921 UUMMANNAQ HELI.	70.68	-52.12	2	
200	GLA00043811 IKERMIUARSSUK	61.93	-42.08	43	GHCN_hourly (Menne et al., 2024)
201	GLA00749128	68.25	-36.50	2925	

https://doi.org/10.5194/essd-2026-449
Preprint. Discussion started: 2 September 2026

	PANORAMANUNATAKKER			
202	GLA00749129 TREKANTNUNATTAKER	69.38	-35.98	2759
203	GLA00749133 NANATAQ	65.07	-40.23	361
204	GLA00749135 KOKLAPPERNE	65.33	-40.30	361
205	GLA00749137 MINT JULEP	66.28	-47.77	829
206	GLA00749138 ICE CAP	68.07	-42.33	593
207	GLA00749139 ICE CAP SITE 2	69.55	-43.17	2559
208	GLA00749145 ICE CAP SITE 3	70.67	-36.17	3140
209	GLA00749146 THULE STE 2	76.53	-68.33	308
210	GLA00749148 ICE CAP SITE 4	78.13	-71.62	0
211	GLA00749149 THULE SITE B	76.00	-56.08	1650
212	GLI0000BGDU DUNDAS	76.50	-69.00	20
213	GLI0000BGGD GROENNEDAL	61.23	-48.10	32
214	GLI0000BGKT CAPE TOBIN (AUT)	70.42	-21.97	41
215	GLI0000BGSS SISIMIUT	66.95	-53.73	50
216	GLI0000BIKA IKATEQ	65.93	-36.68	56
217	GLI0000BMKA MARRAK POINT	63.43	-51.18	41
218	GLM00004165 TO BE DETERMINED	66.48	-46.20	2134
219	GLM00004175 TO BE DETERMINED	65.18	-43.80	2438
220	GLM00004201 TO BE DETERMINED	77.47	-63.22	19
221	GLM00004203 TO BE DETERMINED	76.63	-73.00	11
222	GLM00004208 TO BE DETERMINED	74.03	-57.82	2

https://doi.org/10.5194/essd-2026-449
Preprint. Discussion started: 2 September 2026

223	GLM00004209 UPERNAVIK AWS	72.77	-56.17	63
224	GLM00004216 TO BE DETERMINED	69.22	-51.00	39
225	GLM00004221 TO BE DETERMINED	69.23	-51.07	31
226	GLM00004242 TO BE DETERMINED	65.02	-52.55	14
227	GLM00004266 TO BE DETERMINED	60.77	-48.00	33
228	GLM00004270 TO BE DETERMINED	61.18	-45.40	24
229	GLM00004273 QAQORTOQ HELIPORT	60.72	-46.03	18
230	GLM00004285 TO BE DETERMINED	59.98	-45.20	16
231	GLM00004301 TO BE DETERMINED	83.63	-33.37	2
232	GLM00004365 TO BE DETERMINED	65.53	-37.10	36
233	GLM00004373 TO BE DETERMINED	64.28	-40.30	2
234	GLM00004381 TO BE DETERMINED	61.80	-42.00	33
235	GLM00004418 SUMMIT-US	72.58	-38.50	3198
236	GLM00004436 NEEM	77.50	-50.87	2450
237	GLM00004485 SADDLE	65.98	-44.50	2467
238	GLM00034220 EGEDESMINDE GREENLAND	68.70	-52.87	48
239	GLM00034230 HOLSTEINSBORG GREENLAND	66.93	-53.70	9
240	GLM00034240 SUKKERTOPPEN GREENLAND	65.40	-52.85	26
241	GLM00034250 GODTHAAB GREENLAND	64.17	-51.75	23
242	GLM00034260 FREDERIKSHAAB GREENLAND	62.00	-49.72	16
243	GLM00034310 NORD GREENLAND	81.60	-16.67	36
244	GLM00034320	76.77	-18.77	18

https://doi.org/10.5194/essd-2026-449
Preprint. Discussion started: 2 September 2026

	DANMARKSHAVN GREENLAND			
245	GLM00034330 DANEBORG GREENLAND	74.30	-20.23	7
246	GLM00034349 KANGERDLUGSSUAK GREENLAND	68.15	-31.75	31
247	GLM00034350 APUTITEQ GREENLAND	67.80	-32.27	12
248	GLM00034360 ANGMAGSSALIK GREENLAND	65.60	-37.57	36
249	GLM00034380 TINGMIARMINT GREENLAND	62.53	-42.13	14
250	GLM00034390 PRINCE CHRISTIAN SOUND GREENLA	60.05	-43.20	77
251	GLM00074913 VALKYRIERNE	63.18	-41.33	91
252	GLM00074914 UNGUSIVIK	66.03	-53.7	13
253	GLU0388-001 CEN1	77.18	-61.12	1002
254	GLU0388-016 KPC_UV3	79.84	-25.16	866
255	GLU0388-017 KPC_U	79.83	-25.17	742
256	GLU0388-020 MIT	65.69	-37.90	362
257	GLU0388-021 NAE	75.00	-29.98	382
258	GLU0388-022 NAU	73.84	-49.53	1782
259	GLU0388-023 NEM	77.44	-51.08	1537
260	GLU0388-024 NSE	66.48	-42.49	1969
261	GLU0388-026 NUK_L	64.60	-49.67	440
262	GLU0388-028 NUK_UV3	64.51	-49.28	1113
263	GLU0388-029 NUK_U	64.55	-49.30	832
264	GLU0388-032 QAS_L	61.04	-46.96	239

https://doi.org/10.5194/essd-2026-449
Preprint. Discussion started: 2 September 2026

Open Access Earth System Science Data Discussions

265	GLU0388-033 QAS_M	61.10	-46.83	497
266	GLUHALLEY-2 HALLEY	75.52	-26.00	—
267	GLUHALLEY-3 HALLEY	75.50	-26.00	—
268	GLUHALLEY-4 HALLEY	75.60	-26.00	—
269	GLW00016407 SIMIUTAK	60.69	-46.60	62
270	GLU00004212 UMANAK GREENLAND	70.68	-52.25	7
271	GLM00004217 NAN	68.82	-51.00	76
272	GLM00004207 NAN	81.73	-59.00	105
273	GLM00004351 NAN	67.78	-32.28	2
274	GLM00004382 NAN	61.93	-42.07	2
275	GLM00004218 NAN	69.23	-53.50	24
276	GLU00000054 TAS_L (MOVING ICE STATION)	65.6	-38.90	274
277	GLU00000055 TAS_U (MOVING ICE STATION)	65.70	-38.87	573
278	GLU00000002 CP1 (MOVING ICE STATION)	69.88	-46.98	1960
279	GLU00000003 DY2 (MOVING ICE STATION)	66.48	-46.28	2115
280	GLU00000004 EGP (MOVING ICE STATION)	75.63	-35.98	2653
281	GLU00000005 FRE (MOVING ICE STATION)	74.39	-20.83	688
282	GLU00000006 HUM (MOVING ICE STATION)	78.53	-56.83	1974
283	GLU00000007 JAR (MOVING ICE STATION)	69.50	-49.68	932
284	GLU00000008 KAN_B (MOVING ICE STATION)	67.13	-50.18	350
285	GLU00000009 KAN_L (MOVING ICE STATION)	67.10	-49.93	679
286	GLU00000011	67.00	-47.02	1845

https://doi.org/10.5194/essd-2026-449
Preprint. Discussion started: 2 September 2026

Open Access Earth System Science Data Discussions

	KAN_U (MOVING ICE STATION)			
287	GLU00000012 KPC_L (MOVING ICE STATION)	79.91	-24.09	377
288	GLU00000013 KPC_U (MOVING ICE STATION)	79.83	-25.17	867
289	GLU00000014 LYN_L (MOVING ICE STATION)	69.32	-53.54	540
290	GLU00000015 LYN_T (MOVING ICE STATION)	69.30	-53.59	940
291	GLU00000034 MIT (MOVING ICE STATION)	65.69	-37.83	466
292	GLU00000035 NAE (MOVING ICE STATION)	75.00	-30.00	2623
293	GLU00000036 NAU (MOVING ICE STATION)	73.84	-49.49	2338
294	GLU00000037 NEM (MOVING ICE STATION)	77.44	-51.10	2460
295	GLU00000038 NSE (MOVING ICE STATION)	66.48	-42.50	2372
296	GLU00000039 NUK_B (MOVING ICE STATION)	64.46	-50.15	110
297	GLU00000040 NUK_K (MOVING ICE STATION)	64.16	-51.36	713
298	GLU00000041 NUK_L (MOVING ICE STATION)	64.48	-49.52	585
299	GLU00000042 NUK_N (MOVING ICE STATION)	64.95	-49.88	928
300	GLU00000043 NUK_U (MOVING ICE STATION)	64.50	-49.26	1148
301	GLU00000044 QAS_A (MOVING ICE STATION)	61.25	-46.73	1020
302	GLU00000045 QAS_L (MOVING ICE STATION)	61.02	-46.87	281
303	GLU00000046 QAS_M (MOVING ICE STATION)	61.10	-46.83	626
304	GLU00000047 QAS_U (MOVING ICE STATION)	61.18	-46.82	909
305	GLU00000048 SCO_L (MOVING ICE STATION)	72.23	-26.82	474
306	GLU00000049 SCO_U (MOVING ICE STATION)	72.39	-27.26	994
307	GLU00000050 SDL (MOVING ICE STATION)	66.00	-44.50	2451

https://doi.org/10.5194/essd-2026-449
Preprint. Discussion started: 2 September 2026

Open Access Earth System Science Data Discussions

308	GLU00000051 SDM (MOVING ICE STATION)	63.15	-44.82	2878	
309	GLU00000052 SWC (MOVING ICE STATION)	69.57	-49.31	1149	
310	GLU00000053 TAS_A (MOVING ICE STATION)	65.78	-38.90	897	
311	GLU00000057 THU_L2 (MOVING ICE STATION)	76.39	-68.27	574	
312	GLU00000058 THU_U (MOVING ICE STATION)	76.42	-68.15	765	
313	GLU00000059 TUN (MOVING ICE STATION)	78.02	-33.99	2074	
314	GLU00000060 UPE_L (MOVING ICE STATION)	72.90	-54.30	229	
315	GLU00000061 UPE_U (MOVING ICE STATION)	72.89	-53.54	978	
316	GLU00000056 THU_L (MOVING ICE STATION)	76.40	-68.27	577	
317	Barber	71.68	-38.20	3170	GISP2 (Stearns and Weidner, 1997)
318	Cathy	72.30	-38.00	3210	
319	GISP 2	72.58	-38.46	3205	
320	Julie	72.57	-34.63	3100	
321	Kenton	72.28	-38.80	3185	
322	Klinck	72.35	-40.50	3100	
323	Matt	73.48	-37.62	3100	
324	GRIP	72.57	-37.62	3230	AMRDC (Antarctic Meteorological Research and Data Center, 1989, 1990)
325	Summit (SUM)	72.60	-38.42	3210	NOAA GML
326	0148759 HG	66.33	-38.15	459	NCEI (Holland and Holland, 2016a)
327	0148760 JI	69.22	-49.82	30	NCEI (Holland and Holland, 2016b)

Table A2. Sensor types and measurement accuracy by source.

Source	Sensor	Type	Accuracy
SIGMA	Temperature	Vaisala, HMP155b	±0.17 °C
	Wind Speed	Young, 05103	±0.3 m/s or 1%
	Wind Direction	Young, 05103	±3°
	Relative Humidity	Vaisala, HMP155b	±1% (0% to 90%) ±1.7% (90% to 100%)

https://doi.org/10.5194/essd-2026-449
Preprint. Discussion started: 2 September 2026

	Radiation	Kipp and Zonen, CNR4	(D/USR) ±5% (daily total)
			(D/ULR) ±10% (daily total)
	Pressure	Vaisala, PTB210	±0.30 hPa at 20 °C
	Precipitation	–	–
IMAU	Temperature	Aanderaa 2775C (1993–2001)	0.1 °C at −20 °C
		Vaisala HMP45C (2002–2016)	0.2 °C
	Wind Speed	Aanderaa 2740 (1993–2001)	0.5 m/s
		05103-L R.M. Young (2002–2016)	0.3 m/s
	Wind Direction	Aanderaa 2750 (1993–2001)	5°
		05103-L R.M. Young (2002–2016)	3°
	Relative Humidity	Vaisala HMP35C (1993–2001)	2% (RH < 90%)
		Vaisala HMP45C (2002–2016)	2% (RH < 90%)
	Radiation	Aanderaa 2770	10 W/m^2
	Pressure	Aanderaa 2775C (1993–2001)	0.5 hPa
		Vaisala PTB101B (2002–2016)	0.5 hPa
	Precipitation	–	–
GC-Net Level 1	Temperature	Type-E thermocouple	0.1 °C
		Vaisala 50YC within a Campbell Scientific CS500	0.1 °C
	Wind Speed	RM Young propeller-type vane	0.1 m/s
	Wind Direction	RM Young propeller-type vane	5°
	Relative Humidity	Vaisala INTERCAP 50YC Vaisala HUMICAP HMP45 or HMP155	5% < 90%, 10% > 90%
	Radiation	Kipp & Zonen CG4 Eppley pyrgeometer	4% – 7%
	Pressure	Vaisala PTB101B	0.1 hPa
	Precipitation	–	–
PROMICE	Temperature	Thermometer, aspirated (MP100H-4-1-03-00-10DIN)	±0.1 °C
		Thermometer, aspirated (WS401)	±0.2 °C (−20 to +50 °C), ±0.5 °C (> −30 °C)
		Hygro-/Thermometer, aspirated (HMP155E)	±(0.226 – 0.0028 × temperature) °C
	Wind Speed	Anemometer (05103 or 05105)	±0.2 m/s or ±1% of reading
	Wind Direction	Anemometer (05103 / 05108)	±3°
	Relative Humidity	Hygrometer, aspirated (HygroClip HC2/HC2A-S3)	±0.1 K, ±0.8% RH
		Hygrometer, aspirated (WS401)	±2% RH
		Hygrometer, aspirated (HMP155E)	±0.6% RH (0% – 40%), ±1.0% RH (40% – 95%)
	Radiation	Radiometer (net radiometer,	±10%

		advanced) (CNR1 or CNR4)	
	Pressure	Barometer (CS100 / Setra 278)	±2.0 hPa
		Barometer (digital, integrated) (WS401)	±1.5 hPa, ±0.5 hPa (0 – 40 °C)
	Precipitation	Pluviometer (WS401)	±2.0%
		Rain gauge (T200B)	—
DMI	Temperature	Manual quicksilver thermometer	±0.1 ~ ±0.2 °C
		Aanderaa PT 1000	±(0.15 + 0.002 |T|) °C /± (0.3 + 0.005 |T|) °C
		Vaisala HMP155	-80 ~ +20 °C: ±(0.226 − 0.0028 × T) °C；+20 ~ +60 °C: ±(0.055 + 0.0057 × T) °C
		Vaisala HMP45D	±0.2 °C
	Wind Speed	R.M. Young 05103-5	±0.3 m/s
	Wind Direction	R.M. Young 05103-5	±3°
	Relative Humidity	Vaisala HMP 155	±1% RH (0 – 90% RH，15 – 25 °C); ±1.7% RH (90 – 100% RH)
		Vaisala HMP 45D	±1% RH (0 – 90% RH); ±2% RH (90 – 100% RH)
	Radiation	Campbell Stokes sunshine recorder	±0.1 – 0.2 h
	Pressure	Campbell Scientific CS100 / Setra 278	±0.5 hPa (+20 °C); ±1.0 hPa (0 – 40 °C); ±2.0 hPa (-40 – 60 °C)
	Precipitation	Hellmann rain gauge	–
		Geonor	±0.1%
NCEI	Temperature	Vaisala HMP45C	±0.2 °C
	Wind Speed	Young 05,350	%
	Wind Direction	Young 05,350	3°
	Relative Humidity	Vaisala HMP35C	2% (RH < 90%)
	Radiation	Kipp and zonen CM3 (Pyranometer)	10% day Total
		Kipp and zonen CG3 (Pyrgeometer)	10% day Total
	Pressure	CS105	2 mb
	Precipitation	–	–
GHCN_daily	Temperature	Vaisala HMP155	±0.1 °C
		MMTS electronic thermometer	±0.3 °C
		Air temperature sensor	±0.3 °C
	Wind Speed	Vaisala WMT702	±0.2 m/s / ±2%
		Cup/ultrasonic anemometer	±(0.5 + 0.03 V) m/s
	Wind Direction	Vaisala WMT702	±2°
		Wind vane	±5°

https://doi.org/10.5194/essd-2026-449
Preprint. Discussion started: 2 September 2026

	Relative Humidity	Vaisala HMP155	±1% RH
		Capacitive humidity sensor	±3% RH
	Radiation	Pyranometer	±5%
	Pressure	Digital capacitive barometer	±0.7 hPa
	Precipitation	Heated tipping bucket	±2%
		Vaisala PWD22	
		Standard 8-inch rain gauge	±1%
		Tipping bucket rain gauge	±0.4 mm
GHCN_Hourly	Temperature	Vaisala HMP155	±0.1 ℃
		Thermometrics Platinum Resistance Thermometer	±0.3 ℃
		Platinum Resistance Thermometer	±0.1 ℃
	Wind Speed	Vaisala WMT702	±0.2 m/s / ±2%
		Met One Instruments Model 014A	±0.11 m/s
	Wind Direction	Vaisala WMT702	±2°
	Relative Humidity	Vaisala HMT337	±1% RH
		Capacitive RH sensor	±2% RH
		Vaisala HMP155	±1% RH
	Radiation	Kipp & Zonen SP Lite2 Pyranometer	±5%
	Pressure	Digital capacitive barometer	±0.7 hPa
		Vaisala PTB series	±0.3 hPa
	Precipitation	Heated tipping bucket rain gauge	±2%
GISP2	Temperature	Platinum resistance thermometer	–
	Wind Speed	Belfort cerovane model 123	–
	Wind Direction	–	–
	Relative Humidity	Vaisala HMP-31UT	–
	Radiation	–	–
	Pressure	Parascientific model 215	–
	Precipitation	–	–
AMRDC	Temperature	Platinum resistance thermometer	–
	Wind Speed	Belfort cerovane model 123	–
	Wind Direction	–	–
	Relative Humidity	Vaisala HMP-31UT	–
	Radiation	–	–
	Pressure	Parascientific model 215	–
	Precipitation	–	–
NOAA GML	Temperature	Vaisala HMP45DU	±0.2 ℃
		Vaisala HMP155	±0.1 ℃
	Wind Speed	Vaisala WMT702 Ultrasonic Wind	±0.2 m/s / ±2%

https://doi.org/10.5194/essd-2026-449
Preprint. Discussion started: 2 September 2026

	Sensor	
Wind Direction	Vaisala WMT702 Ultrasonic Wind Sensor	±2°
Relative Humidity	Vaisala HMP45DU	Accuracy (20 °C) ±1% RH Field calibration accuracy: ±2% RH (0 – 90% RH); ±3% RH (90 – 100% RH)
	Vaisala HMP155	±1% RH
Radiation	Precision Spectral Pyranometer (PSP)	Linearity ±0.5%; temperature dependence ±1%
Pressure	Digital Capacitive Barometer	±0.7 hPa
Precipitation	Tipping Bucket Gauge	±2%
	Vaisala PWD22	–

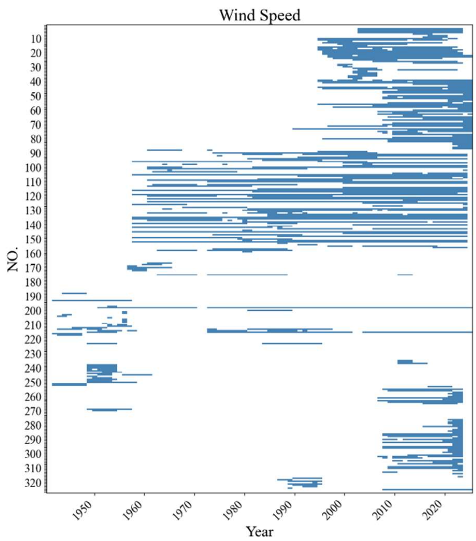

Figure A1. Daily data availability of wind speed. Blue indicates that data is available, and 1–327 correspond to "NO." in Table A1.

https://doi.org/10.5194/essd-2026-449
Preprint. Discussion started: 2 September 2026

Open Access Earth System Science Data Discussions

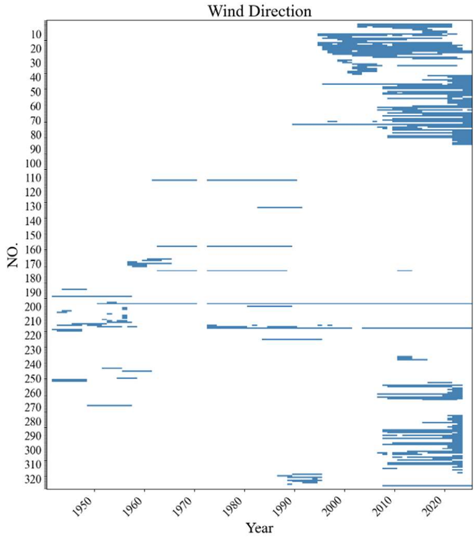

Figure A2. Daily data availability of wind direction. Blue indicates that data is available, and 1–327 correspond to "NO." in Table A1.

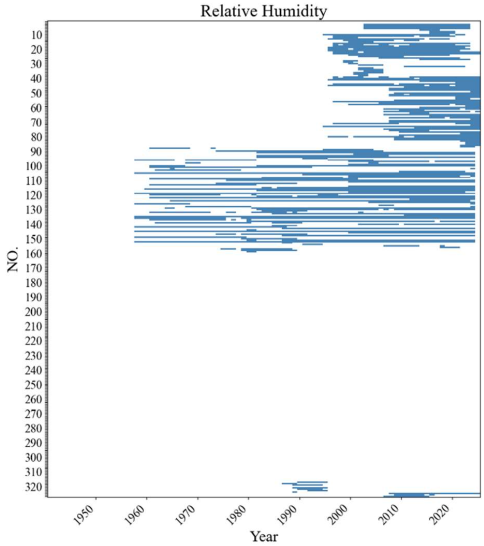

Figure A3. Daily data availability of relative humidity. Blue indicates that data is available, and 1–327 correspond to "NO." in Table A1.

https://doi.org/10.5194/essd-2026-449
Preprint. Discussion started: 2 September 2026

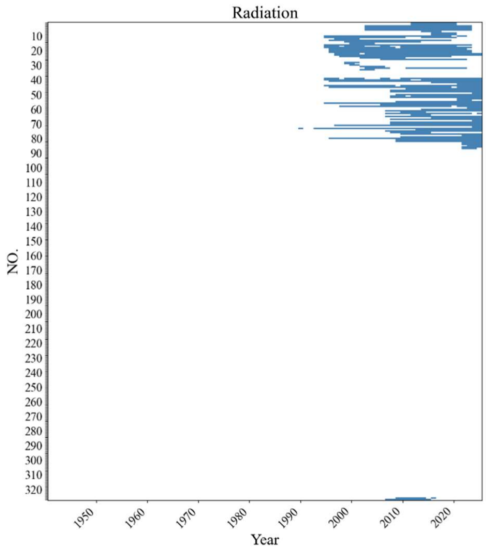

Figure A4. Daily data availability of radiation. Blue indicates that data is available, and 1–327 correspond to "NO." in Table A1.

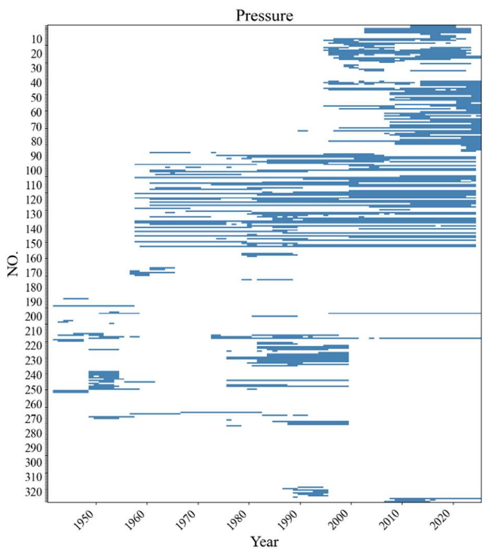

Figure A5. Daily data availability of pressure. Blue indicates that data is available, and 1–327 correspond to "NO." in Table A1.

https://doi.org/10.5194/essd-2026-449
Preprint. Discussion started: 2 September 2026

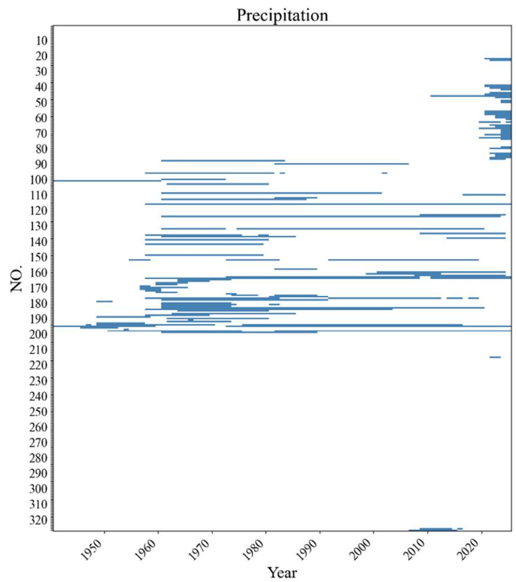

Figure A6. Daily data availability of precipitation. Blue indicates that data is available, and 1–327 correspond to "NO." in Table A1.

Text.A1 Parameter configurations of the LSTM-CNN

The model applies MinMaxScaler for normalization, then extracts local features through two one-dimensional convolutional layers, each with a ReLU activation function. To prevent overfitting, two Dropout layers were applied after the LSTM layer for regularization. During training, the mean squared error (MSE) is used as the loss function, and the Adam optimizer was applied with an initial learning rate of 10−3 and a weight decay of 10−5. The learning rate scheduling employs the ReduceLROnPlateau strategy, halving the learning rate if the validation loss fails to decrease for five consecutive epochs. Concurrently, an early stopping mechanism is implemented to terminate training when the validation loss shows no improvement for ten consecutive epochs, with a maximum training cycle limit set at 300. To ensure experimental reproducibility, a unified random seed is configured across all stages.

Text.A2 Parameter configurations of the Transformer-CNN

The input data is normalized using StandardScaler in this model. Both fully connected layers and convolutional layers in the model employ the ReLU activation function. Dropout layers are incorporated to enhance model generalization. The Adam optimizer is used during training with a learning rate of 1e−3. The loss function is MSE, while Mean Absolute Error (MAE) is monitored as an evaluation metric.

https://doi.org/10.5194/essd-2026-449
Preprint. Discussion started: 2 September 2026

An early stopping mechanism is implemented during training: training terminates and optimal weights are restored when the validation set loss fails to improve for 20 consecutive epochs. The maximum number of training epochs is set to 100, with a batch size of 32.

Text.A3 Parameter configurations of the SoftRandomForest

Both input features and target variables were normalized using the StandardScaler method. A soft decision tree was firstly defined by specifying the dimensions of the input features and the tree depth. The initial depth was set to 3, yielding 2 depth−1 internal nodes and 2 depth leaf nodes. To construct a soft random forest model based on a soft decision tree, a forest of 10 trees, each with depth 3, was implemented. Each tree was trained independently, and its predictors were calculated. The outputs of all trees were stacked into a new tensor, and their average was taken as the final prediction.

Text.A4 Parameter configurations of the SoftXGBoost

The pre-processing steps were identical to those of SoftRandomForest, and the model was constructed using the same definition of a soft decision tree. The model learning rate was set to 0.1, and each tree in the forest was traversed to obtain the predicted value, which was multiplied by the learning rate and then summed to gradually accumulate the contribution of each tree to the final output. Ten models were trained independently for 300 epochs each, using the Criterion loss function to calculate and evaluate discrepancies between predicted and target values.

Text.A5 Parameter configurations of the ANN

Before training, both input and target variables were standardized separately using StandardScaler to remove the scale and range differences across variables. To consider observatory site representativeness, weights are assigned to each station by calculating the histogram difference between the distribution of station data and that of the whole study area, ensuring that the model can better reflect the large-scale characteristics (Vandecrux et al., 2024). The ANN consisted of three hidden layers, each containing 250 neurons with the ReLU activation function. The output layer had a single neuron for predicting the target variable. In addition, a Gaussian noise layer was added to the input layer to enhance robustness. The model was trained using the Adam optimizer with RMSE as loss function, over 250 epochs with a batch size of 3000.

Code and data availability

Greenland weather station observation dataset is available at https://doi.org/10.11888/Atmos.tpdc.303490. (Wang and Wang, 2026). Users are encouraged to cite the original product references provided in the accompanying 'Station Information.csv' file, in addition to citing this paper. Reconstructed monthly SAT data are available at https://doi.org/10.11888/Cryos.tpdc.303026. (Wang and Wang, 2025). ERA5 and ERA5-land data are available at https://cds.climate.copernicus.eu/. The code for the artificial neural network model used for temperature reconstruction in Greenland can be found at https://doi.org/10.5281/zenodo.8027442 (Vandecrux, 2023) and is distributed under the GNU General Public License version 2.0 (GPL-2.0). The code for the additional machine learning models used for reconstruction and the code for processing the observational data are available at https://doi.org/10.5281/zenodo.21714043 and https://doi.org/10.5281/zenodo.21713966, respectively, and both are distributed under the MIT License.

Author contributions

SW and YW conceived this work. SW developed the methodology, prepared the figures and tables using the compiled and reconstructed data. YW supervised this work. SW prepared the original draft, which was reviewed and edited by YW, and further improved by YZ, ZZ and SH.

Competing interests.

All authors have declared that neither of them has any conflicts of interest.

Acknowledgements

We sincerely thank the following institutions and researchers for generously providing data support: the Global Historical Climatology Network (GHCN), the Danish Meteorological Institute, the PROMICE and GC-Net projects, the NOAA National Centers for Environmental Information for archiving the GISP2 ice core climate data from the Greenland Summit, the NOAA Global Monitoring Laboratory for providing the in situ observations at Summit, the Antarctic Meteorological Research and Data Center for releasing the GRIP observational dataset, and the PANGAEA data publishing platform. Special thanks go to Smeets et al. (2018) and Van Tiggelen et al. (2024a, b) for sharing their compiled automatic weather station temperature data, to Nishimura et al. (2023) for publishing the high-quality meteorological dataset from the SIGMA automatic weather station in northwestern Greenland, to Holland and Holland (2016a, b) for providing the automatic weather station data from the Jakobshavn and Helheim glacier ice fronts, and to Fan et al. (2022) for providing Greenland elevation data. The open sharing of these data resources has provided abundant observational support for this study, making the research more scientifically robust.

Financial support

This study was financially supported by National Key Research and Development Program of China (2020YFA0608202), the National Natural Science Foundation of China (41971081), and Shanghai Frontiers Science Center of Polar Science (SOO2024-06).

References

Adolph, A. C., Albert, M. R., and Hall, D. K.: Near-surface temperature inversion during summer at summit, greenland, and its relation to MODIS-derived surface temperatures, Cryosphere, 12, 907–920, https://doi.org/10.5194/tc-12-907-2018, 2018.

Antarctic Meteorological Research and Data Center: GRIP automatic weather station, greenland, 1989 reader format three-hour observational data [data set], https://doi.org/10.48567/3WM7-YN10, 1989.

Antarctic Meteorological Research and Data Center: GRIP automatic weather station, greenland, 1990 reader format three-hour observational data [data set], https://doi.org/10.48567/SDM4-DF26, 1990.

Beckmann, J. and Winkelmann, R.: Effects of extreme melt events on ice flow and sea level rise of the Greenland Ice Sheet, Cryosphere, 17, 3083–3099, https://doi.org/10.5194/tc-17-3083-2023, 2023.

Biau, G. and Scornet, E.: A random forest guided tour, Test, 25, 197–227, https://doi.org/10.1007/s11749-016-0481-7, 2016.

Bonsoms, J., Oliva, M., López-Moreno, J. I., and Fettweis, X.: Rising Extreme Meltwater Trends in Greenland Ice Sheet (1950–2022): Surface Energy Balance and Large-Scale Circulation Changes, J. Clim., 37, 4851–4866, https://doi.org/10.1175/JCLI-D-23-0396.1, 2024.

Box, J. E., Yang, L., Bromwich, D. H., and Bai, L.-S.: Greenland Ice Sheet Surface Air Temperature Variability: 1840–2007, J. Clim., 22, 4029–4049, https://doi.org/10.1175/2009JCLI2816.1, 2009.

Box, J. E., Hubbard, A., Bahr, D. B., Colgan, W. T., Fettweis, X., Mankoff, K. D., Wehrlé, A., Noël, B., Van Den Broeke, M. R., Wouters, B., Bjørk, A. A., and Fausto, R. S.: Greenland ice sheet climate disequilibrium and committed sea-level rise, Nat. Clim. Change, 12, 808–813, https://doi.org/10.1038/s41558-022-01441-2, 2022.

Breiman, L.: Random forests, Mach. Learn., 45, 5–32, https://doi.org/10.1023/A:1010933404324, 2001.

Brenning, A.: Spatial cross-validation and bootstrap for the assessment of prediction rules in remote sensing: the R package sperrorest, in: 2012 IEEE International Geoscience and Remote Sensing Symposium, IGARSS 2012 - 2012 IEEE International Geoscience and Remote Sensing Symposium, 5372–5375, https://doi.org/10.1109/IGARSS.2012.6352393, 2012.Che, J., Ding, M., Zhang, Q., Wang, Y., Sun, W., Wang, Y., Wang, L., and Huai, B.: Reconstruction of near-surface air temperature over the Greenland ice sheet based on MODIS data and machine learning approaches, Remote Sens., 14, 5775, https://doi.org/10.3390/rs14225775, 2022.

Chen, T. and Guestrin, C.: XGBoost: a scalable tree boosting system, arXiv:1603.02754 [cs], 785–794, https://doi.org/10.1145/2939672.2939785, 2016.

Christiansen, B. and Ljungqvist, F. C.: Challenges and perspectives for large-scale temperature reconstructions of the past two millennia, Rev. Geophys., 55, 40–96, https://doi.org/10.1002/2016RG000521, 2017.

Colosio, P., Tedesco, M., Fettweis, X., and Ranzi, R.: Surface melting over the Greenland ice sheet from enhanced resolution passive microwave brightness temperatures (1979–2019), https://doi.org/10.5194/tc-2020-250, 21 September 2020.

Covi, F., Hock, R., Rennermalm, Å., Fettweis, X., and Noël, B.: Spatiotemporal variability of air temperature biases in regional climate models over the Greenland ice sheet, J. Glaciol., 71, e64, https://doi.org/10.1017/jog.2025.38, 2025.

Cowtan, K. and Way, R. G.: Coverage bias in the HadCRUT4 temperature series and its impact on recent temperature trends, Q. J. R. Meteorolog. Soc., 140, 1935–1944, https://doi.org/10.1002/qj.2297, 2014.

Cox, C. J., Noone, D. C., Berkelhammer, M., Shupe, M. D., Neff, W. D., Miller, N. B., Walden, V. P., and Steffen, K.: Supercooled liquid fogs over the central greenland ice sheet, Atmos. Chem. Phys., 19, 7467–7485, https://doi.org/10.5194/acp-19-7467-2019, 2019.

Cybenko, G.: Approximation by superpositions of a sigmoidal function, Math. Control Signals Syst., 2, 303–314, https://doi.org/10.1007/BF02551274, 1989.

Danish Meteorological Institute (DMI): Weather Observations from Greenland 1958-2024 - Observational data with description, DMI Report 25-08, Danish Meteorological Institute, Copenhagen, https://www.dmi.dk/publikationer/, 2025.

Fan, Y., Ke, C.-Q., and Shen, X.: A new Greenland digital elevation model derived from ICESat-2 during 2018–2019, Earth Syst. Sci. Data, 14, 781–794, https://doi.org/10.5194/essd-14-781-2022, 2022.

Fausto, R. S., How, P., Vandecrux, B., Lund, M. C., Box, J. E., Mankoff, K. D., Andersen, S. B., Van As, D., Bahbah, R., Citterio, M., Colgan, W., Jakobsgaard, H. T., Karlsson, N. B., Kjeldsen, K. K., Larsen, S. H., Olsen, C., Oraschewski, F. M., Rutishauser, A., Shields, C. L., Solgaard, A. M., Stevens, I. T., Svendsen, S. H., Langley, K., Messerli, A., Bjørk, A. A., Andersen, J. K., Abermann, J., Steiner, J., Prinz, R., Hynek, B., Lea, J. M., Brough, S., and Ahlstrøm, A. P.: PROMICE | GC-NET automatic weather station data, Earth Syst. Sci. Data, 18, 2829–2873, https://doi.org/10.5194/essd-18-2829-2026, 2026.

Golledge, N. R., Keller, E. D., Gomez, N., Naughten, K. A., Bernales, J., Trusel, L. D., and Edwards, T. L.: Global environmental consequences of twenty-first-century ice-sheet melt, Nature, 566, 65–72, https://doi.org/10.1038/s41586-019-0889-9, 2019.

Gorter, W., Van Angelen, J. H., Lenaerts, J. T. M., and Van Den Broeke, M. R.: Present and future near-surface wind climate of Greenland from high resolution regional climate modelling, Clim. Dyn., 42, 1595–1611, https://doi.org/10.1007/s00382-013-1861-2, 2014.

Guy, H., Brooks, I. M., Turner, D. D., Cox, C. J., Rowe, P. M., Shupe, M. D., Walden, V. P., and Neely, R. R.: Observations of fog-aerosol interactions over central greenland, J. Geophys. Res.: Atmos., 128, e2023JD038718, https://doi.org/10.1029/2023JD038718, 2023.

Hanna, E., Cappelen, J., Fettweis, X., Mernild, S. H., Mote, T. L., Mottram, R., Steffen, K., Ballinger, T. J., and Hall, R. J.: Greenland surface air temperature changes from 1981 to 2019 and implications for ice-sheet melt and mass-balance change, Int. J. Climatol., 41, E1336–E1352, https://doi.org/10.1002/joc.6771, 2021.

Hersbach, H., Bell, B., Berrisford, P., Hirahara, S., Horányi, A., Muñoz-Sabater, J., Nicolas, J., Peubey, C., Radu, R., Schepers, D., Simmons, A., Soci, C., Abdalla, S., Abellan, X., Balsamo, G., Bechtold, P., Biavati, G., Bidlot, J., Bonavita, M., De Chiara, G., Dahlgren, P., Dee, D., Diamantakis, M., Dragani, R., Flemming, J., Forbes, R., Fuentes, M., Geer, A., Haimberger, L., Healy, S., Hogan, R. J., Hólm, E., Janisková, M., Keeley, S., Laloyaux, P., Lopez, P., Lupu, C., Radnoti, G., De Rosnay, P., Rozum, I., Vamborg, F., Villaume, S., and Thépaut, J.: The ERA5 global reanalysis, Q. J. R. Meteorolog. Soc., 146, 1999–2049, https://doi.org/10.1002/qj.3803, 2020.

Hochreiter, S. and Schmidhuber, J.: Long short-term memory, Neural Comput., 9, 1735–1780, https://doi.org/10.1162/neco.1997.9.8.1735, 1997.

Holland, D. M. and Holland, D.: AIR TEMPERATURE, RELATIVE HUMIDITY, and others collected from automatic weather station installed on rock outcrop in helheim glacier ice front from 2009-08-11 to 2016-02-20 (NCEI accession 0148759) [data set], 2016a.

Holland, D. M. and Holland, D.: AIR TEMPERATURE, RELATIVE HUMIDITY, and others collected from automatic weather station installed on rock outcrop in jakobshavn glacier ice front from 2007-10-13 to 2016-02-14 (NCEI accession 0148760) [data set], 2016b.

Hornik, K., Stinchcombe, M., and White, H.: Multilayer feedforward networks are universal approximators, Neural Networks, 2, 359–366, https://doi.org/10.1016/0893-6080(89)90020-8, 1989.

Hou, J., Wang, Y., Hou, B., Zhou, J., and Tian, Q.: Spatial simulation and prediction of air temperature based on CNN-LSTM, Appl. Artif. Intell., 37, 2166235, https://doi.org/10.1080/08839514.2023.2166235, 2023.

How, P., Lund, M. C., Ahlstrøm, A. P., Andersen, S. B., Box, J. E., Citterio, M., Colgan, W. T., Fausto, R. S., Karlsson, N. B., Jakobsen, J., Jakobsgaard, H. T., Larsen, S. H., Mankoff, K. D., Nielsen, R. B., Rutishauser, A., Shield, C. L., Solgaard, A. M., Stevens, I. T., van As, D., Vandecrux, B., Abermann, J., Bjørk, A. A., Langley, K., Lea, J., Messerli, A., and Prinz, R.: PROMICE and GC-net automated weather station data in Greenland [data set], https://doi.org/10.22008/FK2/IW73UU, 2022.

Huai, B., Van Den Broeke, M. R., and Reijmer, C. H.: Long-term surface energy balance of the western Greenland ice sheet and the role of large-scale circulation variability, Cryosphere, 14, 4181–4199, https://doi.org/10.5194/tc-14-4181-2020, 2020.

Huang, J., Zhang, X., Zhang, Q., Lin, Y., Hao, M., Luo, Y., Zhao, Z., Yao, Y., Chen, X., Wang, L., Nie, S., Yin, Y., Xu, Y., and Zhang, J.: Recently amplified arctic warming has contributed to a continual global warming trend, Nature Clim Change, 7, 875–879, https://doi.org/10.1038/s41558-017-0009-5, 2017.

IPCC: Climate Change 2021: The Physical Science Basis. Contribution of Working Group I to the Sixth Assessment Report of the Intergovernmental Panel on Climate Change [Masson-Delmotte, V., Zhai, P., Pirani, A., Connors, S. L., Péan, C., Berger, S., Caud, N., Chen, Y., Goldfarb, L., Gomis, M. I., Huang,

https://doi.org/10.5194/essd-2026-449
Preprint. Discussion started: 2 September 2026

M., Leitzell, K., Lonnoy, E., Matthews, J. B. R., Maycock, T. K., Waterfield, T., Yelekçi, O., Yu, R., and Zhou, B. (eds.)], Cambridge University Press, Cambridge, United Kingdom and New York, NY, USA, doi:10.1017/9781009157896, 2021.

Jammalamadaka, S. R. and SenGupta, A.: Topics in circular statistics, WORLD SCIENTIFIC, https://doi.org/10.1142/4031, 2001.

John Cappelen (ed): Greenland - DMI Historical Climate Data Collection 1784-2013, Danish Meteorological Institute, Copenhagen, 2014.

Johnstone, C. and Sulungu, E. D.: Application of neural network in prediction of temperature: a review, Neural Comput. Appl., 33, 11487–11498, https://doi.org/10.1007/s00521-020-05582-3, 2021.

Karpatne, A., Ebert-Uphoff, I., Ravela, S., Babaie, H. A., and Kumar, V.: Machine Learning for the Geosciences: Challenges and Opportunities, IEEE Trans. Knowl. Data Eng., 31, 1544–1554, https://doi.org/10.1109/TKDE.2018.2861006, 2019.

Kawaguchi, K., Shakespeare, C. J., and Roderick, M. L.: CO2 dependence in global estimation of all-sky downwelling longwave: parameterization and model comparison, Geophys. Res. Lett., 51, e2024GL110384, https://doi.org/10.1029/2024GL110384, 2024.

Konzelmann, T. and Braithwaite, R. J.: Variations of ablation, albedo and energy balance at the margin of the Greenland ice sheet, kronprins christian land, eastern north Greenland, J. Glaciol., 41, 174–182, https://doi.org/10.3189/S002214300001786X, 1995.

Lenton, T. M., Held, H., Kriegler, E., Hall, J. W., Lucht, W., Rahmstorf, S., and Schellnhuber, H. J.: Tipping elements in the Earth's climate system, Proc. Natl. Acad. Sci., 105, 1786–1793, https://doi.org/10.1073/pnas.0705414105, 2008.

Lenton, T. M., Rockström, J., Gaffney, O., Rahmstorf, S., Richardson, K., Steffen, W., and Schellnhuber, H. J.: Climate tipping points — too risky to bet against, Nature, 575, 592–595, https://doi.org/10.1038/d41586-019-03595-0, 2019.

Li, D., Folini, D., and Wild, M.: Assessment of top of atmosphere, atmospheric and surface energy budgets in CMIP6 models on regional scales, Earth Space Sci., 10, e2022EA002758, https://doi.org/10.1029/2022EA002758, 2023.

Li, Q., Wang, C., An, L., and Ding, M.: Influence of supraglacial lakes on accuracy of inversion of Greenland ice sheet surface melt data in different passive microwave bands, Remote Sens., 16, 1673, https://doi.org/10.3390/rs16101673, 2024.

Ma, Z., Huang, J., Zhang, X., Luo, Y., Dou, T., and Ding, M.: Deep learning-based reconstruction of monthly antarctic surface air temperatures from 1979 to 2023, Sci. Data, 12, 847, https://doi.org/10.1038/s41597-025-05175-6, 2025.

Menne, M., Noone, S., Casey, N., Dunn, R., McNeill, S., Kantor, D., Thorne, P. W., Orcutt, K., Cunningham, S., and Risavi, N.: Global historical climatology network-hourly (GHCNh), version 1 [data set], https://doi.org/10.25921/JP3D-3V19, 2024.

Menne, M. J., Durre, I., Vose, R. S., Gleason, B. E., and Houston, T. G.: An overview of the global historical climatology network-daily database, J. Atmos. Oceanic Technol., 29, 897–910, https://doi.org/10.1175/JTECH-D-11-00103.1, 2012a.

Menne, M. J., Durre, I., Korzeniewski, B., McNeill, S., Thomas, K., Yin, X., Anthony, S., Ray, R., Vose, R. S., Gleason, B. E., and Houston, T. G.: Global historical climatology network - daily (GHCN-daily), version 3 [data set], https://doi.org/10.7289/V5D21VHZ, 2012b.

Muñoz-Sabater, J., Dutra, E., Agustí-Panareda, A., Albergel, C., Arduini, G., Balsamo, G., Boussetta, S., Choulga, M., Harrigan, S., Hersbach, H., Martens, B., Miralles, D. G., Piles, M., Rodríguez-Fernández, N. J., Zsoter, E., Buontempo, C., and Thépaut, J.-N.: ERA5-land: a state-of-the-art global reanalysis dataset for land applications, Earth Syst. Sci. Data, 13, 4349–4383, https://doi.org/10.5194/essd-13-4349-2021, 2021.

Mutiibwa, D., Strachan, S., and Albright, T.: Land surface temperature and surface air temperature in complex terrain, IEEE J. Sel. Top. Appl. Earth Obs. Remote Sens., 8, 4762–4774, https://doi.org/10.1109/jstars.2015.2468594, 2015.

Nishimura, M., Aoki, T., Niwano, M., Matoba, S., Tanikawa, T., Yamaguchi, S., Yamasaki, T., Tsushima, A., Fujita, K., Iizuka, Y., and Kurosaki, Y.: Quality-controlled datasets of automatic weather station (AWS) at SIGMA-A site from 2012 to 2020: level 1.3 (2.00) [data set], https://doi.org/10.17592/001.2022041303, 2023a.

Nishimura, M., Aoki, T., Niwano, M., Matoba, S., Tanikawa, T., Yamaguchi, S., Yamasaki, T., and Fujita, K.: Quality-controlled datasets of automatic weather station (AWS) at SIGMA-B site from 2012 to 2020: level 1.3 (2.00) [data set], https://doi.org/10.17592/001.2022041306, 2023b.

Nishimura, M., Aoki, T., Niwano, M., Matoba, S., Tanikawa, T., Yamasaki, T., Yamaguchi, S., and Fujita, K.: Quality-controlled meteorological datasets from SIGMA automatic weather stations in

https://doi.org/10.5194/essd-2026-449
Preprint. Discussion started: 2 September 2026

northwest Greenland, 2012–2020, Earth System Science Data, 15, 5207–5226, https://doi.org/10.5194/essd-15-5207-2023, 2023c.

Noël, B., Van Kampenhout, L., Lenaerts, J. T. M., Van De Berg, W. J., and Van Den Broeke, M. R.: A 21st century warming threshold for sustained greenland ice sheet mass loss, Geophys. Res. Lett., 48, e2020GL090471, https://doi.org/10.1029/2020GL090471, 2021.

Przybylak, R., Singh, G., Wyszyński, P., Araźny, A., and Chmist, K.: Air temperature changes in SW Greenland in the second half of the 18th century, Clim. Past, 20, 1451–1470, https://doi.org/10.5194/cp-20-1451-2024, 2024.

Rapp, D., Vinther, B. M., Høyer, J. L., Jensen, C. D., and Scheller, J. H.: Sampling biases in daily average temperatures from Greenland climate records, Int. J. Climatol., 46, e70317, https://doi.org/10.1002/joc.70317, 2026.

Rasmussen, L. H., Markussen, B., and Ditlevsen, S.: A pan-arctic terrestrial in situ weather dataset from 1990-2023 collected from publicly available data sources, Sci. Data, 12, 1242, https://doi.org/10.1038/s41597-025-05441-7, 2025.

Rasmussen, R., Baker, B., Kochendorfer, J., Meyers, T., Landolt, S., Fischer, A. P., Black, J., Thériault, J. M., Kucera, P., Gochis, D., Smith, C., Nitu, R., Hall, M., Ikeda, K., and Gutmann, E.: How well are we measuring snow: the NOAA/FAA/NCAR winter precipitation test bed, Bull. Am. Meteorol. Soc., 93, 811–829, https://doi.org/10.1175/BAMS-D-11-00052.1, 2012.

Rolland, C.: Spatial and seasonal variations of air temperature lapse rates in alpine regions, J. Clim., 16, 1032–1046, https://doi.org/10.1175/1520-0442(2003)016<1032:SASVOA>2.0.CO;2, 2003.

Sherstinsky, A.: Fundamentals of recurrent neural network (RNN) and long short-term memory (LSTM) network, Physica D, 404, 132306, https://doi.org/10.1016/j.physd.2019.132306, 2020.

Smeets, P. C. J. P., Kuipers Munneke, P., Van As, D., Van Den Broeke, M. R., Boot, W., Oerlemans, H., Snellen, H., Reijmer, C. H., and Van De Wal, R. S. W.: The K-transect in west Greenland: automatic weather station data (1993–2016), Arct., Antarc., Alp. Res., 50, https://doi.org/10.1080/15230430.2017.1420954, 2018.

Smeets, P. C. J. P., van den Broeke, M. R., Boot, W., Cover, G., Eijkelboom, M., Greuell, W., Tijm-Reijmer, C. H., Snellen, H., and van de Wal, R. S. W.: Automatic weather station data collected from 2003 to 2021 at the Greenland ice sheet along the K-transect, west-greenland [data set], https://doi.org/10.1594/PANGAEA.947483, 2022.

Stearns, C. R. and Weidner, G. A.: NOAA/WDS paleoclimatology - GISP2 ice core automatic weather station data [data set], https://doi.org/10.25921/2BY8-T941, 1997.

Stearns, C. R., Weidner, G. A., and Keller, L. M.: Atmospheric circulation around the Greenland crest, J. Geophys. Res.: Atmos., 102, 13801–13812, https://doi.org/10.1029/96JD03360, 1997.

Steffen, K., Vandecrux, B., Houtz, D., Abdalati, W., Bayou, N., Box, J. E., Colgan, W. T., Espona Pernas, L., Griessinger, N., Haas-Artho, D., Heilig, A., Hubert, A., Iosifescu Enescu, I., Johnson-Amin, N., Karlsson, N. B., Kurup Buchholz, R., McGrath, D., Cullen, N. J., Naderpour, R., Molotch, N. P., Pedersen, A. Ø., Perren, B., Philipps, T., Plattner, G.-K., Proksch, M., Revheim, M. K., Særrelse, M., Schneebli, M., Sampson, K., Starkweather, S., Steffen, S., Stroeve, J., Watler, B., Winton, Ø. A., Zwally, J., and Ahlstrøm, A.: GC-net level 1 historical automated weather station data [data set], https://doi.org/10.22008/FK2/VVXGUT, 2022.

Szymanowski, M. and Kryza, M.: The role of auxiliary variables in deterministic and deterministic-stochastic spatial models of air temperature in Poland, Pure Appl. Geophys., 174, 595–621, https://doi.org/10.1007/s00024-015-1199-2, 2017.

The IMBIE Team: Mass balance of the Greenland ice sheet from 1992 to 2018, Nature, 579, 233–239, https://doi.org/10.1038/s41586-019-1855-2, 2020.

Van Tiggelen, M., Smeets, P. C. J. P., Reijmer, C. H., van As, D., Box, J. E., Fausto, R. S., Khan, S. A., Rignot, E., and van den Broeke, M. R.: Daily surface energy balance (SEB) and quality-controlled meteorological quantities measured at 19 stations on the Greenland ice sheet (2003-2023) [data set], https://doi.org/10.1594/PANGAEA.970127, 2024a.

Van Tiggelen, M., Smeets, P. C. J. P., Tijm-Reijmer, C. H., Miège, C., Forster, R. R., Khan, S. A., Rignot, E., and van den Broeke, M. R.: Hourly automatic weather station data collected on zachariae isstrøm, northeast-greenland (2016-2020) and at a firn aquifer site, east Greenland (2014-2017) [data set], https://doi.org/10.1594/PANGAEA.971647, 2024b.

Vandecrux, B.: Greenland ice sheet subsurface temperature compilation script [code], https://doi.org/10.5281/ZENODO.8027442, 2023.

Vandecrux, B., Box, J. E., Ahlstrøm, A. P., Andersen, S. B., Bayou, N., Colgan, W. T., Cullen, N. J., Fausto, R. S., Haas-Artho, D., Heilig, A., Houtz, D. A., How, P., Iosifescu Enescu, I., Karlsson, N. B., Kurup Buchholz, R., Mankoff, K. D., McGrath, D., Molotch, N. P., Perren, B., Revheim, M. K., Rutishauser, A., Sampson, K., Schneebeli, M., Starkweather, S., Steffen, S., Weber, J., Wright, P. J.,

https://doi.org/10.5194/essd-2026-449
Preprint. Discussion started: 2 September 2026

Zwally, H. J., and Steffen, K.: The historical greenland climate network (GC-net) curated and augmented level-1 dataset, Earth Syst. Sci. Data, 15, 5467–5489, https://doi.org/10.5194/essd-15-5467-2023, 2023.

Vandecrux, B., Fausto, R. S., Box, J. E., Covi, F., Hock, R., Rennermalm, Å. K., Heilig, A., Abermann, J., Van As, D., Bjerre, E., Fettweis, X., Smeets, P. C. J. P., Kuipers Munneke, P., Van Den Broeke, M. R., Brils, M., Langen, P. L., Mottram, R., and Ahlstrøm, A. P.: Recent warming trends of the Greenland ice sheet documented by historical firn and ice temperature observations and machine learning, Cryosphere, 18, 609–631, https://doi.org/10.5194/tc-18-609-2024, 2024.

Vaswani, A., Shazeer, N., Parmar, N., Uszkoreit, J., Jones, L., Gomez, A. N., Kaiser, L., and Polosukhin, I.: Attention is all you need, https://doi.org/10.48550/ARXIV.1706.03762, 2017.

Von Storch, H., Zorita, E., Jones, J. M., Dimitriev, Y., González-Rouco, F., and Tett, S. F. B.: Reconstructing past climate from noisy data, Science, 306, 679–682, https://doi.org/10.1126/science.1096109, 2004.

Wang, S. and Wang, Y.: Monthly SAT at the resolution of 0.1°×0.1° across the Greenland during 1950-2024 National Tibetan Plateau / Third Pole Environment Data Center [data set], https://doi.org/10.11888/Cryos.tpdc.303026, 2025.

Wang, S., Wang, Y.: A Greenland weather station observation dataset. National Tibetan Plateau / Third Pole Environment Data Center [data set], https://doi.org/10.11888/Atmos.tpdc.303490. https://cstr.cn/18406.11.Atmos.tpdc.303490, 2026.

Wang, Y., Zhang, X., Ning, W., Lazzara, M. A., Ding, M., Reijmer, C. H., Smeets, P. C. J. P., Grigioni, P., Heil, P., Thomas, E. R., Mikolajczyk, D., Welhouse, L. J., Keller, L. M., Zhai, Z., Sun, Y., and Hou, S.: The AntAWS dataset: a compilation of antarctic automatic weather station observations, Earth Syst. Sci. Data, 15, 411–429, https://doi.org/10.5194/essd-15-411-2023, 2023.

Yu, Y., Si, X., Hu, C., and Zhang, J.: A review of recurrent neural networks: LSTM cells and network architectures, Neural Comput., 31, 1235–1270, https://doi.org/10.1162/neco_a_01199, 2019.

Zhang, W., Wang, Y., Smeets, P. C. J. P., Reijmer, C. H., Huai, B., Wang, J., and Sun, W.: Estimating near-surface climatology of multi-reanalyses over the Greenland ice sheet, Atmos. Res., 259, 105676, https://doi.org/10.1016/j.atmosres.2021.105676, 2021.

Zhao, B., Lu, H., Chen, S., Liu, J., and Wu, D.: Convolutional neural networks for time series classification, J. Syst. Eng. Electron., 28, 162–169, https://doi.org/10.21629/jsee.2017.01.18, 2017.

https://doi.org/10.5194/essd-2026-449
Preprint. Discussion started: 2 September 2026

Zwally, H.J., Giovinetto, M.B., Beckley, M.A., Saba, J.L: Antarctic and Greenland Drainage Systems. GSFC Cryospheric Sciences Laboratory. https://earth.gsfc.nasa.gov/cryo/data/polar-altimetry/antarctic-and-greenland-drainage-systems (accessed on 7 February 2024), 2012.